Ocean Systems Engineering, *Vol. 14, No. 2 (2024) 171-210*
https://doi.org/10.12989/ose.2024.14.2.171

Mooring chain fatigue analysis of a deep draft semi-submersible platform in central Gulf of Mexico

Jun Zou*

Floating and Green Energy Consulting, LLC, Houston, Texas, USA

(Received April 23 2024, Revised June 17, 2024, Accepted June 20, 2024)

Abstract. This paper focuses on the rigorous and holistic fatigue analysis of mooring chains for a deep draft semi-submersible platform in the challenging environment of the central Gulf of Mexico (GoM). Known for severe hurricanes and strong loop/eddy currents, this region significantly impacts offshore structures and their mooring systems, necessitating robust designs capable of withstanding extreme wind, wave and current conditions. Wave scatter and current bin diagrams are utilized to assess the probabilistic distribution of waves and currents, crucial for calculating mooring chain fatigue. The study evaluates the effects of Vortex Induced Motion (VIM), Out-of-Plane-Bending (OPB), and In-Plane-Bending (IPB) on mooring fatigue, alongside extreme single events such as 100-year hurricanes and loop/eddy currents including ramp-up and ramp-down phases, to ensure resilient mooring design. A detailed case study of a deep draft semi-submersible platform with 16 semi-taut moorings in 2,500 meters of water depth in the central GoM provides insights into the relative contributions of wave scatter diagram, VIMs from current bin diagram, the combined stresses of OPB/IPB/TT and extreme single events. By comparing these factors, the study aims to enhance understanding and optimize mooring system design for safety, reliability, and cost-effectiveness in offshore operations within the central GoM. The paper addresses a research gap by proposing a holistic approach that integrates findings from various contributions to advance current practices in mooring design. It presents a comprehensive framework for fatigue analysis and design optimization of mooring systems in the central GoM, emphasizing the critical importance of considering environmental conditions, OPB/IPB moments, and extreme single events to ensure the safety and reliability of mooring systems for offshore platforms.

Keywords: extreme single events; fatigue; Out-of-Plane-Bending (OPB) and In-Plane-Bending (IPB); mooring chain; vortex induced motion; wave scatter diagram

1. Introduction

Semi-submersible platforms possess unique attributes ideal for offshore operations. They offer stability and seamless integration with quayside facilities, ensuring operational efficiency even in harsh sea-states. Their expansive deck area accommodates modular or integrated topsides, facilitating future expansions with minimal impact on construction, transportation, and installation processes.

According to D'Souza *et al.* (2019), the global floating production platforms comprises over three hundred units, with semisubmersible Floating Production Systems (FPS) and Floating

*Corresponding author, Ph.D., E-mail: jun.zou@fg-energies.com

http://www.techno-press.org/?journal=ose&subpage=7 ISSN: 2093-6702 (Print), 2093-677X (Online)

Production Storage and Offloading Platforms (FPSOs) constituting the majority. This widespread adoption underscores their versatility and effectiveness in various offshore environments worldwide, including the challenging conditions of the Gulf of Mexico and other deepwater regions.

The global oil and gas industry is increasingly exploring deep and ultra-deepwater reservoirs in key regions such as the Gulf of Mexico (GoM), Offshore Brazil, Offshore Western Australia, and Offshore Mexico to meet rising energy demands worldwide. In water depths exceeding 2,000 meters, tension leg platforms (TLPs) become cost-prohibitive due to engineering and logistical challenges, while Spar platforms require complex offshore hull and deck integration and installation processes.

The metocean conditions in the central Gulf of Mexico are notably demanding, characterized by severe environments prone to hurricanes and robust eddy currents. This study focuses on analyzing these extreme conditions to design resilient mooring systems capable of withstanding intense hurricanes and strong eddy currents impacting offshore structures.

D'Souza *et al.* (2024) documented the evolution of deepwater semi-submersible Floating Production Platform (FPS) mooring systems in the Gulf of Mexico (GoM). They provided comprehensive data on mooring systems deployed on seventeen semi-submersibles installed in the GoM up to the first quarter of 2024. Over the years, water depths have significantly increased, ranging from 470 meters for the Placid platform in 1988 to 2420 meters for the Independence Hub platform in 2007.

Mooring patterns have evolved in line with technological advancements, transitioning from traditional chain-wire-chain configurations to more robust chain-polyester-chain setups. Additionally, mooring equipment has advanced from on-vessel tensioners and chain jacks to advanced off-vessel tensioners (OVT), first employed by Kings Quay starting production in 2022, and in-line tensioners (ILT), introduced by Vito with production commencing in 2023.

Mooring chain diameters have also varied significantly, ranging from 75 mm for platforms like GOMEZ in 2006 to 171mm for Mad Dog 2, renamed Argos in 2023. These developments reflect ongoing efforts in the offshore industry to enhance the reliability and operational capabilities of mooring systems in deepwater environments.

The mooring system of a semi-submersible platform consists of clusters of mooring lines crucial for maintaining stationkeeping across various sea states, ensuring specified offset limits are adhered to. The failure of a mooring line can have severe consequences, including production shutdown, riser damage leading to hydrocarbon pollution, and potential loss of life.

Gordon *et al.* (2014) conducted a thorough review spanning from 2000 to 2013, incorporating studies by Ma *et al.* (2013), Sai and D'Souza (2013), and Kvitrud (2013). They identified multiple root causes of mooring failures, including tension overload, tension-tension (TT) fatigue, out-of-plane bending (OPB) induced fatigue, excessive wear and corrosion, and manufacturing defects. Fatigue-related issues, notably TT fatigue and OPB fatigue, account for 25% or more of mooring failures.

Given the critical implications of mooring failures, there is an urgent need to develop a comprehensive and holistic method for fatigue assessment during the mooring system design phase. This approach intends to proactively address and mitigate the likelihood of failures throughout the service life of offshore structures. By integrating advanced fatigue assessment techniques and drawing insights from past failures, the offshore industry can enhance the reliability and safety of mooring systems, thereby minimizing operational risks and ensuring long-term operational integrity.

TT fatigue analysis, crucial for assessing long-term operational conditions, typically employs a wave scatter diagram representing numerous sea states. Each sea state includes waves, wind, and currents from different directions with associated probabilities of occurrence. In the Gulf of Mexico

(GoM), a distinctive feature is the presence of strong loop eddy currents. Therefore, TT fatigue analysis must also consider fatigue induced by VIM.

VIM occurs when a slender object in a uniform flow sheds vortices downstream, oscillating transversely if the shedding frequency aligns with the platform's transverse natural frequency. This phenomenon is prominent in Spar platforms, well-documented in API RP 2SK (2008) and studies by Zou *et al.* (2011). Deep draft semi-submersible platforms also experience VIM, as observed in studies by Gonçalves *et al.* (2012), Zou *et al.* (2013), Zou (2014), and subsequent research.

Given its significant impact on mooring and riser strength and fatigue, understanding VIM characteristics is crucial for mooring system design and analysis. Due to its complex structural-hydrodynamic interaction, model testing plays a pivotal role in investigating VIM physics. These tests derive Max A/D and Normal A/D envelopes, alongside drag coefficients, establishing VIM design curves as a vital consideration in offshore platform design.

Out-of-Plane Bending (OPB) fatigue in mooring chains, initially identified in the Girassol Loading Buoy in 2001, revealed a distinct failure mechanism compared to traditional tension-tension (TT) fatigue. This discovery prompted the establishment of a Joint Industry Project (JIP) spanning from 2007 to 2013. The OPB JIP yielded significant insights into OPB physics through comprehensive testing, contributing valuable data on interlink stiffness and stress concentration factors.

The findings from the Chain OPB JIP were instrumental in developing guidelines as summarized in the Bureau Veritas guidelines (2014). Rampi *et al.* (2015) and subsequent publications (2016 a, b, c) further emphasized critical lessons learned from the OPB JIP. Izadparast *et al.* (2018) expanded on these insights, providing a guidance note that outlines key aspects of chain OPB fatigue analysis, offering practical value to the industry. Chung *et al.* (2020) employed a multi-scale approach in their study. They acquired mooring tension and interlink angle data near the chain stopper through global-system time-domain simulation. For chains, fatigue was assessed using a more intricate Finite Element Method (FEM) analysis. Their use of time-dependent tension and interlink angle data as inputs for the fatigue analysis showcased a sophisticated analytical methodology.

Collectively, these efforts have enhanced understanding and methodologies for mitigating OPB fatigue in mooring systems, thereby improving the reliability and durability of offshore structures in challenging offshore environments.

The significance of potential fatigue damage from extreme single events was prominently recognized in API RP 2T (2010), specifically for Tension Leg Platform (TLP) tendon components. This standard stressed the necessity of assessing tendon fatigue induced by extreme single events to ensure tendon (vertical mooring) durability.

Interestingly, mooring components for semi-submersible platforms under ABS (2023) and DNV (2015 and 2016) guidelines were not mandated to undergo checks for fatigue induced by extreme single events. Nonetheless, considering such assessments would enhance the robustness of mooring design, ensuring it can withstand extreme conditions and unexpected events effectively.

By incorporating evaluations for extreme single event-induced fatigue, designers can bolster the reliability and durability of mooring systems, reinforcing safety standards and mitigating risks in offshore operations.

To date, numerous studies have investigated VIM and OPB/IPB induced mooring fatigue individually. However, there is a notable gap in research focusing on a holistic approach that evaluates these factors along with contributions from wave scatter diagrams, and the impact of extreme single events like 100-year hurricanes and loop/eddy currents.

Our study targets to address this gap by providing insights into how each factor - VIM, OPB/IPB, wave and current characteristics, and extreme single events - affects mooring chain fatigue. By identifying the governing factors through this holistic approach, we seek to enhance understanding and optimize mooring system design for increased reliability and performance in challenging offshore environments like the central Gulf of Mexico.

Through this research, we aim to contribute valuable knowledge to the field and establish a framework that includes diverse environmental and operational factors into mooring system fatigue analysis, ensuring robust and effective design practices for offshore structures.

The structure of the paper includes detailed case studies, metocean criteria, numerical models, key input data considerations, comprehensive analysis results, discussions on findings, and practical recommendations. By synthesizing these elements, this study intends to enhance current mooring design practices and contribute to the development of robust mooring systems capable of withstanding the demanding offshore conditions of the central GoM.

2. Mooring fatigue analysis methodologies

The study employs time-domain coupled analysis as the method, capturing nonlinear aspects of extreme mooring line tension. This approach explicitly models moorings and risers using finite element methods, integrating their responses with hull motions. Key parameters such as mooring and riser stiffness, mass, damping, hydrodynamic added mass, and drag are explicitly included to simulate their effects on hull response. Coupled analysis thus accounts for dynamic mooring and riser influences on overall platform responses.

Following the acquisition of mooring line tension time series, fatigue damage due to each bin is computed using rain flow counting and either TN or SN-curves (DNV SN curve for TT fatigue and BV SN curve for the combined stress fatigue), depending on whether TT fatigue or the combined stress fatigue is analyzed. Methodologies for TT fatigue and combined stress fatigue are detailed in Section 2.1 and Section 2.2, respectively. Fracture mechanics analysis of mooring fatigue is excluded from this study.

2.1 Tension-tension fatigue analysis methodology

For tension-tension (TT) fatigue analysis, there are two primary methods used to assess mooring fatigue: the tension-cycle (TN) approach, as outlined in API-RP-2SK (2005), and the stress-cycle (SN) approach, as defined in DNV-OS-E301 (2015).

2.1.1 Tension-tension fatigue per TN curve

The chain fatigue damage per TN curve (API-RP-2SK, 2005) can be expressed as,

$$D = N * \left(2^{1/2} * R_{rms} \right)^{m} * \Gamma(1 + m/2) / K \tag{1}$$

In Eq. (1), N, number of cycles; R_{rms}, the ratio of tension range to the reference mooring breaking strength; m, the slope of T-N curve; K, the intercept of the T-N curve. Both m and K values depend on the type of components. For this study, studless chain, m=3, K= 316 were considered. Higher K value based on vendor fatigue test might be allowed to apply per class society's approval.

2.1.2 Tension-tension fatigue per SN curve

The chain fatigue damage per SN curve (DNV OS-E301, 2021) can be written as

$$n_c(s) = a_D s^{-m} \tag{2}$$

The Eq. (2) can be linearized and recast in logarithm format below

$$\log(n_c(s)) = \log(a_D) - m\log(s) \tag{3}$$

In Eq. (2), $n_c(s)$, number of stress ranges (number of cycles); s, stress range (double amplitude) in MPa; a_D, the intercept of the S-N curve; m, the slope of S-N curve. The parameter a_D and m for studless chain, m=3.0, $a_D = 6.0*10^{10}$ were applied for this study.

2.1.3 Resultant fatigue damages

The accumulated fatigue damage for each mooring line from all bins can be calculated using equations specified in API RP 2SK (Eq. (1)) or DNV OS-E301 (Eq. (2)), denoted as

$$D = \sum_{i=1}^{n} D_i \tag{4}$$

In Eq. (4), n: total number of bins; D: total accumulated fatigue damages.

2.1.4 Minimum safety factor

Regardless of whether TN curve or SN curve was employed for tension-tension fatigue damage calculation, the minimum safety factor is 10.

2.2 The combined stress fatigue analysis methodology

The use of OVT as interface components between mooring top chains and the hull is illustrated in Fig. 1. The interlink moment formula was presented in BV guidelines (2014) which was derived from least square method using OPB JIP test data (Melis *et al*. 2005, Rampi and Vargas 2006). For detailed formulas and methodologies, please refer to the BV guidelines (2014).

2.2.1 Interlink angle

In Fig. 1, the FPS hull undergoes rotational motions, with the main housing connecting to the foundation of the OVT fixed on the FPS hull. A vertical rotation pin allows the entire OVT mooring tensioner to rotate in the horizontal plane. Additionally, a latch housing connects to the main housing via a horizontally oriented pin, permitting vertical movement of the latch housing.

Chain link #0 is rigidly connected to the chain stopper, and chain link #1's upper end connects to the lower end of chain link #0, which is mounted on the chain stopper. The lower end of chain link #1 is outside the chain stopper and freely connects to the upper end of chain link #2. The interlink angle between chain link #1 and chain link #2 is expected to be the largest, corresponding to the highest OPB moment. The interlink angle decreases sequentially from one link to the next, becoming negligible after 20 links.

From Fig. 1, calculating the interlink angle becomes complex due to the interaction of chain links (beginning from chain link #1 downwards) influenced by the latch housing, capable of vertical

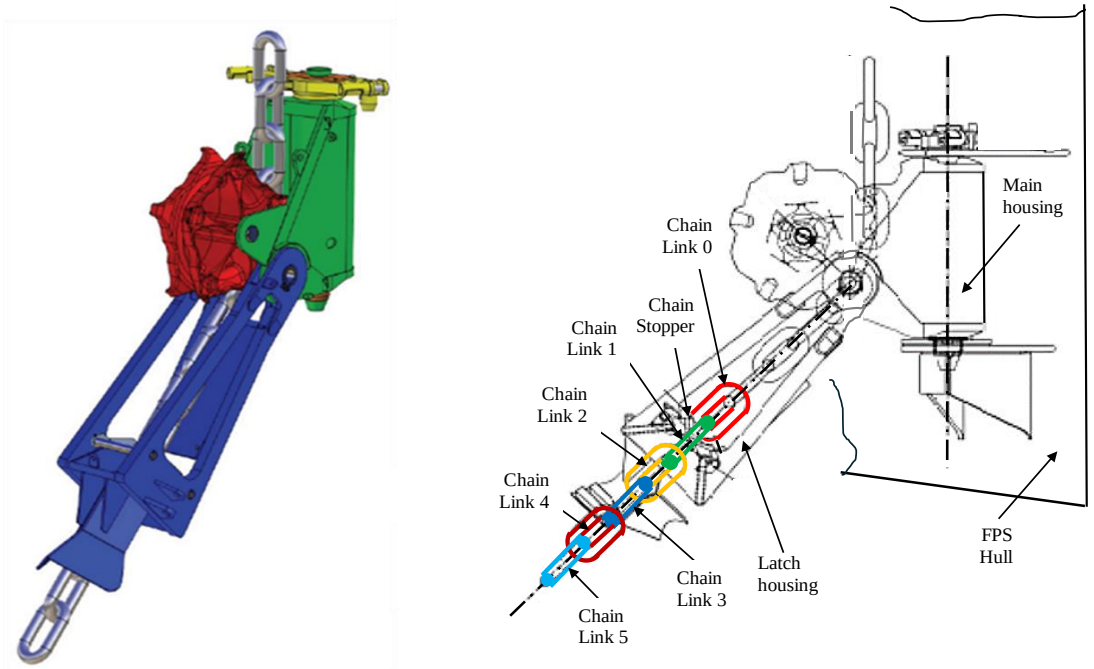

(a) A sample off-vessel-tensioner (OVT, Bardex)

(b) Schematic connection between OVT and FPS hull and top chain link numbering

Fig. 1 A sample OVT, schematic connection of OVT and FPS hull and top chain link numbering

movement. The latch housing is connected to the main housing, allowing horizontal movement, while the main housing links to the FPS hull, which experiences 6-DOF motions.

Certain mechanical components feature specified or designed friction coefficients, applicable to both the vertical and horizontal pins. These components are designed to slide if subjected to in-plane or out-of-plane bending moments that exceed their specified limits. The sticking or sliding behaviors of the OVT significantly impact the calculation of the interlink angle. Further details on establishing numerical models are discussed and revealed in Section 5, Numerical modeling.

2.2.2 OVT sliding moment limits

As depicted in Fig. 1, there are two pins situated within their respective bearings: one vertical pin positioned on the OVT foundation, with the main housing connected to it, and the other horizontal pin linking the main housing to the latch housing. The dimensions of these pins and their specified friction coefficients are carefully designed to ensure they possess adequate loading capacities. This design is crucial for effectively mitigating OPB and IPB moments, thereby preventing OPB/IPB-induced fatigue from becoming the dominant factor in mooring fatigue analysis.

The sliding moment limit formula per BV guidelines (2014) has been slightly modified to be suitable for both pins as follows

$$M_{lim_i} = 0.55\ \mu_i D_i F_i \tag{5}$$

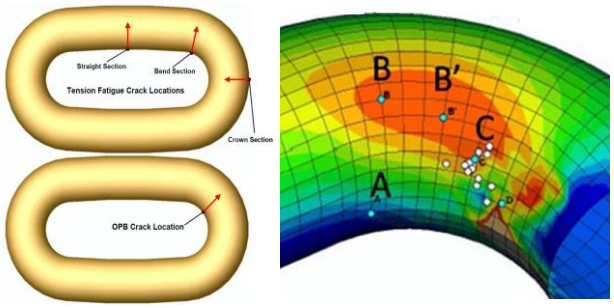

(a) Illustration of hot spots (OTC-25779-MS)

Locations	Descriptions	Remakrs
A	Starting of bending area inner side	No OPB
B	Potential maximum combined stress due to TT, OPB and IPB	Uniaxial OPB
B'	Potential maximum combined stress due to TT, OPB and IPB	Uniaxial OPB
C	Potential maximum combined stress due to TT, OPB and IPB closer to contact area	Multi-axial OPB

(b) Description of hot spots

Fig. 2 Locations of hot spots on a chain link

Table 1 Stress Concentration Factors (BV guidelines, 2014)

Loading modes	Locations of hot spots			
	A	B	B’	C
TT	4.48	2.08	1.65	1.04
OPB	0.00	1.06	1.15	$1.21\gamma_{TT}{}^{*}$
IPB	1.25	0.71	0.66	1.50

γ_{TT} is the mean stress correction factor which can be calculated by Eq. (6) below.

In Eq. (5), M_{lim} is sliding moment limit; “i” is pin number indicator, i=1 represents the vertical pin and i=2 stands for horizontal pin; μ is friction coefficient, μ_1 is friction coefficient at vertical pin location and μ_2 is friction coefficient at horizontal pin location; D is diameter of the pin in the bearing, D_1 is the diameter of the vertical pin and D_2 is the diameter of the horizontal pin; F is the instantaneous loading on pin, F_1 is the instantaneous loading on the vertical pin and F_2 is the instantaneous loading on the horizontal pin.

The friction coefficients in Eq. (5) typically derive from vendor prototype breakout tests, with typical values ranging from 0.05 to 0.15. Notably, the friction coefficients between two adjacent chains are considerably higher, typically around 0.5 in air and 0.3 in seawater

2.2.3 Hot spots and stress concentration factors

There are four typical hot spots on a chain link as displayed in Fig. 2 and corresponding stress concentration factors at these four hot spots (BV guidelines, 2014) are summarized in Table 1.

$$\gamma_{TT} = 1 + 0.9\left(\frac{P}{MBL} - 0.15\right) \tag{6}$$

In Eq. (6), P is mooring line pretension in kN and MBL stands for mooring line breaking strength in kN. γ_{TT} is not less than 0.95.

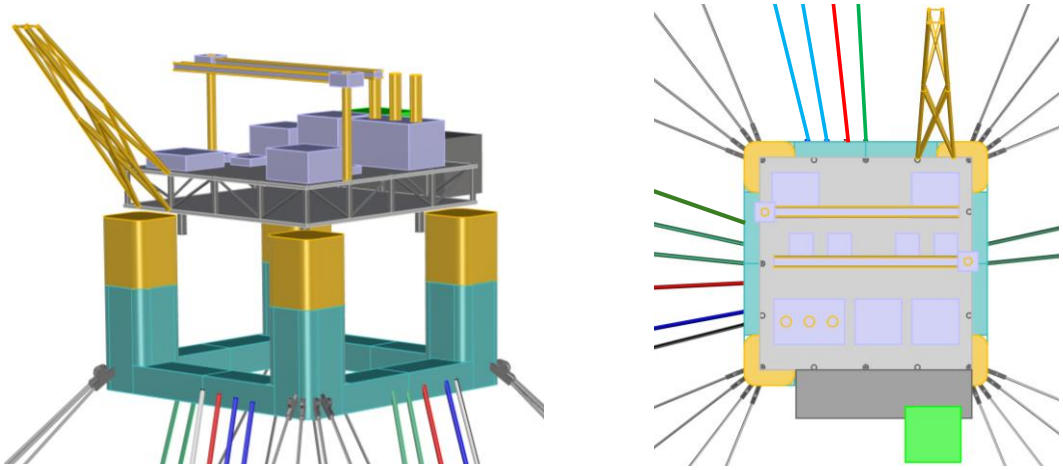

(a) DD semi platform – perspective view (b) DD semi platform – top view

Fig. 3 A generic DD semi platform with 16 moorings and 12 SCRs

2.2.4 Calculation of the combined stresses

To ensure the worst stress combination on a chain link captured, at each location (A, B, B' and C), four possible combinations of stresses due to TT, OPB and IPB per BV guidelines (2014) are given in the formula below

$$\Delta\sigma_{combined} = Z_{corr}(\Delta\sigma_{TT} \pm Z_s\Delta\sigma_{OPB} \pm Z_s\Delta\sigma_{IPB}) \quad (7)$$

In Eq. (7), Z_{corr} is 1.08 and Z_s is 1.06. $\Delta\sigma_{TT}$, $\Delta\sigma_{OPB}$ and $\Delta\sigma_{IPB}$ can be calculated by formula given in BV guidelines (2014).

2.2.5 SN curve for the combined fatigue calculation

SN curve for the combined fatigue calculation (BV Guidelines, 2014) is reproduced as follows,

$$K = N\Delta\sigma_{combined}{}^{m} \quad (8)$$

In Eq. (8), K and m for the single slope design SN curve in sea water under free corrosion, log K = 12,575 and m = 3.

2.2.6 Minimum safety factor for the combined fatigue

For single slope free corrosion SN-curve (Eq. (8)) the minimum safety factor is 3 (BV, 2014).

3. Description of study case

3.1 Overview of the deep draft semisubmersible platform

Key parameter design data of a generic deep draft four-column ring pontoon semisubmersible (DD semi) with topsides payloads 25,000 mt, 16 mooring lines and 12 steel catenary risers (SCRs) in central GoM in 2,500 m with 25-year service life are depicted in Fig. 3 and presented in Table 2.

Table 2 Key Parameter Design Data

Platform displacement (mt)	87,000
Platform draft (m)	35.0
Topside payloads (mt)	25,000
Still water clearance to bottom of lower deck (m)	26.0
SCRs vertical loads (mt)	5,500
Mooring vertical loads (mt)	4,350

Table 3 Particulars of the Deep Draft Semi-submersible Hull

Column center-to-center span (m)	75.0
Square column with round corner (m)	19.5 x 19.5
Column freeboard from MWL to TOC (m)	22.5
Deck post height (m)	3.5
Still water clearance to bottom of lower deck (m)	26.0
Hull draft (m)	35.0
Column height (m)	57.5
Pontoon height (m) x equivalent width (m)	9.5 x 15.5

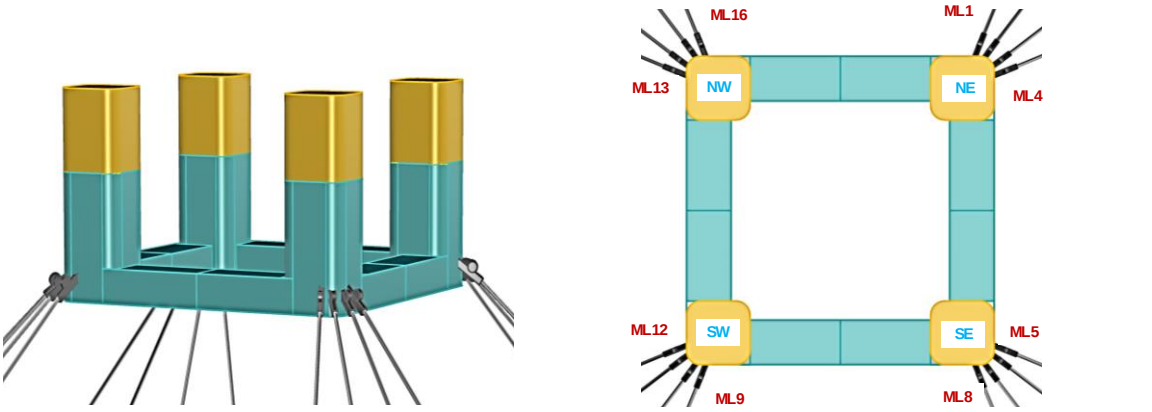

(a) DD semi hull – perspective view (b) DD semi hull – top view and mooring line numbering

Fig. 4 A generic DD semi hull with 16 mooring lines

3.2 Deep draft semisubmersible hull configuration

The deep draft semisubmersible hull configuration is illustrated in Fig. 4 and its principal dimensions of hull configuration are summarized in Table 3.

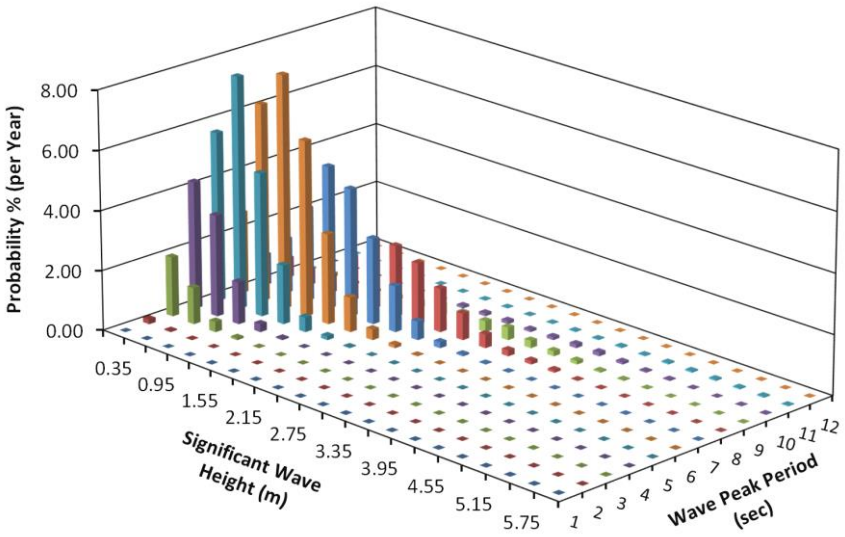

Fig. 5 Distributions of significant wave heights and wave peak periods

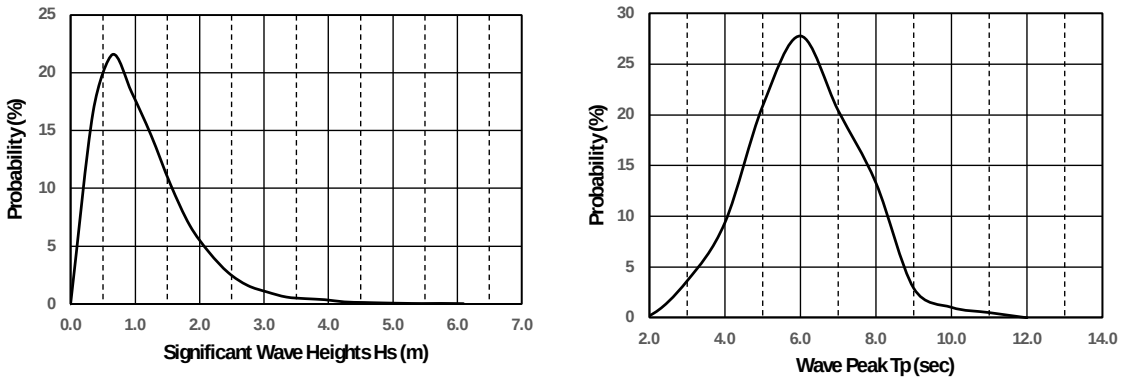

(a) Probabilities of significant wave heights (b) Probabilities of wave peak periods

Fig. 6 Probabilities of significant wave heights and wave peak periods

3.3 Mooring configuration

As displayed in Fig. 4, there are 16 moorings in 4x4 pattern and 4 lines in each cluster. The angle between adjacent lines in the same cluster is 5 degrees apart. Mooring line numbering starts from Northeast (NE) column cluster and increases clock wisely, ML 1 to ML 16. The mooring composition is chain-polyester-chain and mooring configuration is summarized in Table 4.

3.4 SCRs layout and vertical Loads

There are 12 SCRs as illustrated in Fig. 3 which include one oil export, one gas export, five oil productions, three gas injections and two water injections. The resultant vertical loads are 5,500 mt.

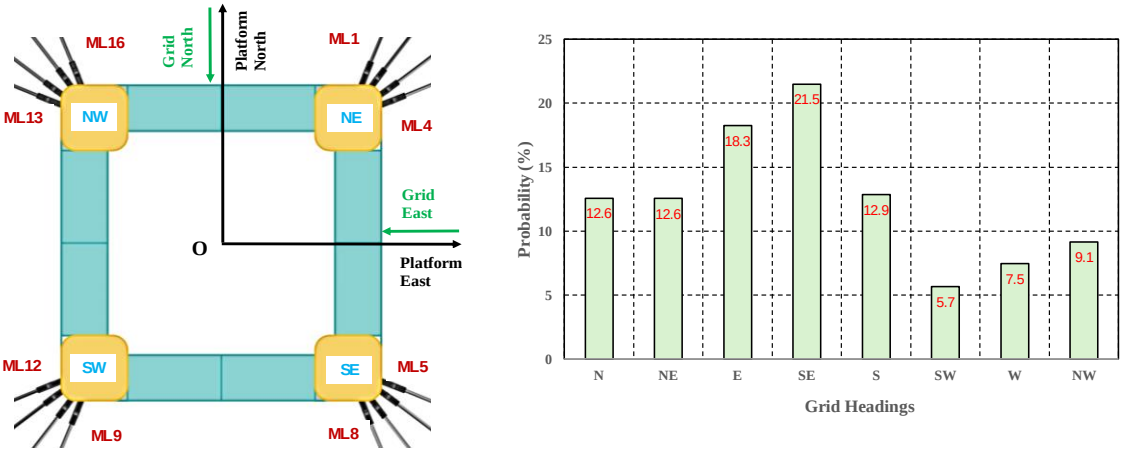

(a) Grid heading definition and platform coordinate system

(b) Probabilities of significant wave heights vs grid headings

Fig. 7 Grid heading definition, platform coordinate system and probabilities of significant wave heights vs grid headings

4. Generic metocean criteria

4.1 Overview

The wave scatter diagram, defined as the joint probability of significant wave height (Hs) and representative period (Tz or Tp) according to API RP 2MET (2021), is crucial for assessing wave-induced mooring fatigue. Current bins utilized in this study align with those detailed in Zou (2014). Peak values of single events, such as 100-year hurricanes and loop currents, are scaled up in accordance with API RP 2MET (2021) guidelines. Further discussions on these topics are elaborated in Sections 4.2 to 4.5, respectively.

4.2 Wave scatter diagram

Detailed wave scatter diagram data are documented in API RP 2MET (2021) and are illustrated in Fig. 5. The distributions of significant wave height and wave peak period are depicted in Fig. 6. As API RP 2MET (2021) does not specify wave significant height vs. directions, typical distributions of significant wave heights vs. headings in central GoM were assumed and presented in Fig. 8 for this study.

From Figs. 5 and 6, the highest probability of significant wave height is approximately 0.75 meters, and the highest probability of wave peak period is around 6.0 seconds. Fig. 7 indicates that the highest probability of waves originates from the grid Southeast.

4.3 Current distribution bins

The current distribution bins used in this study align with those in Zou (2014). In the Gulf of Mexico (GoM), annual loop current occurrences vary significantly across different zones: 46 days

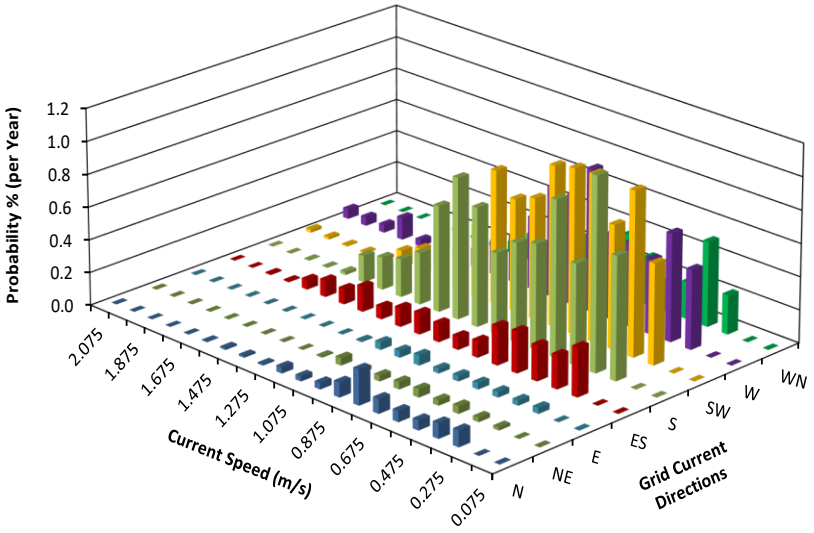

Fig. 8 Distributions of current speeds and grid current directions

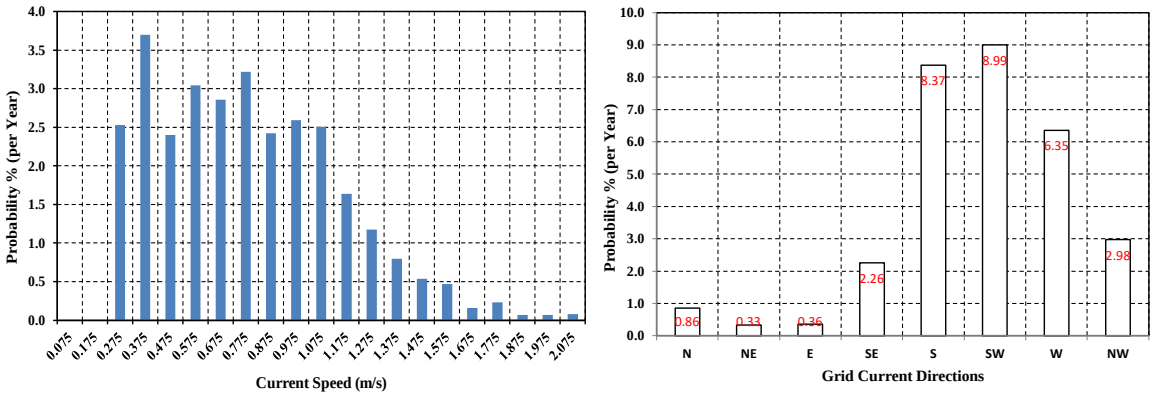

(a) Probabilities of current speeds (b) Probabilities of grid current directions

Fig. 9 Probabilities of current speeds and grid current directions

in benign, 84 days in medium, and 112 days in severe zones. This study focuses on the severe loop current region. For simplicity, 16 grid current directions were consolidated into 8 grid current headings and are depicted in Figs. 8 and 9 respectively.

From Figs. 8 and 9, the highest probability of current speed is 0.375 m/s, and the predominant current direction is from the grid Southwest.

4.4 Single event - 100-year hurricanes

A generic central GoM single event 100-year hurricane 48 hours of ramping-up, reaching peak and ramping-down wave, wind, and current data are summarized in Table 5 and plotted in Fig. 10.

Table 5 A Generic Central GoM Single Event: 100-year Hurricanes

Single Event Bins	Hours From Peak (hrs)	100-year Hs (m)	100-year Tp (s)	Hourly wind (m/s)	Surface current (m/s)
1	-24	3.09	8.87	15.75	0.67
2	-22	3.33	9.09	16.21	0.69
3	-20	3.65	9.41	16.91	0.72
4	-18	4.07	9.73	17.73	0.76
5	-16	4.60	10.17	18.78	0.79
6	-14	5.24	10.71	19.60	0.83
7	-12	5.94	11.25	20.41	0.87
8	-10	6.86	11.79	22.28	0.94
9	-8	8.01	12.55	25.20	1.06
10	-6	9.42	13.30	29.16	1.24
11	-4	11.26	14.17	34.06	1.45
12	-2	13.69	15.25	39.31	1.67
13	0	15.80	16.01	46.08	1.95
14	2	14.06	15.36	42.34	1.79
15	4	12.04	14.49	37.56	1.60
16	6	10.52	13.85	34.65	1.47
17	8	9.44	13.30	32.20	1.36
18	10	8.47	12.76	29.75	1.26
19	12	7.72	12.33	27.30	1.16
20	14	7.22	12.01	25.20	1.06
21	16	6.79	11.79	23.21	0.98
22	18	6.42	11.57	21.35	0.91
23	20	6.07	11.25	20.30	0.86
24	22	5.72	11.03	19.25	0.81
25	24	5.38	10.82	18.20	0.77

In Fig. 10, hourly wind speeds were scaled down by factor of 3 and current speeds were scaled up by factor of 5.

4.5 Single event - 100-year loop currents

In API RP 2MET (2021), the highest 100-year loop current speed in central GoM is 2.75 m/s. A generic central GoM single event 100-year loop current 252 hours of ramping-up, reaching peak and ramping-down surface current speed data are presented in Tables 6a, 6b and 6c and plotted/displayed in Figs. 11(a) and 11(b) respectively.

Per API RP 2MET (2021), loop current profile and associated wind and waves are specified in Table 7.

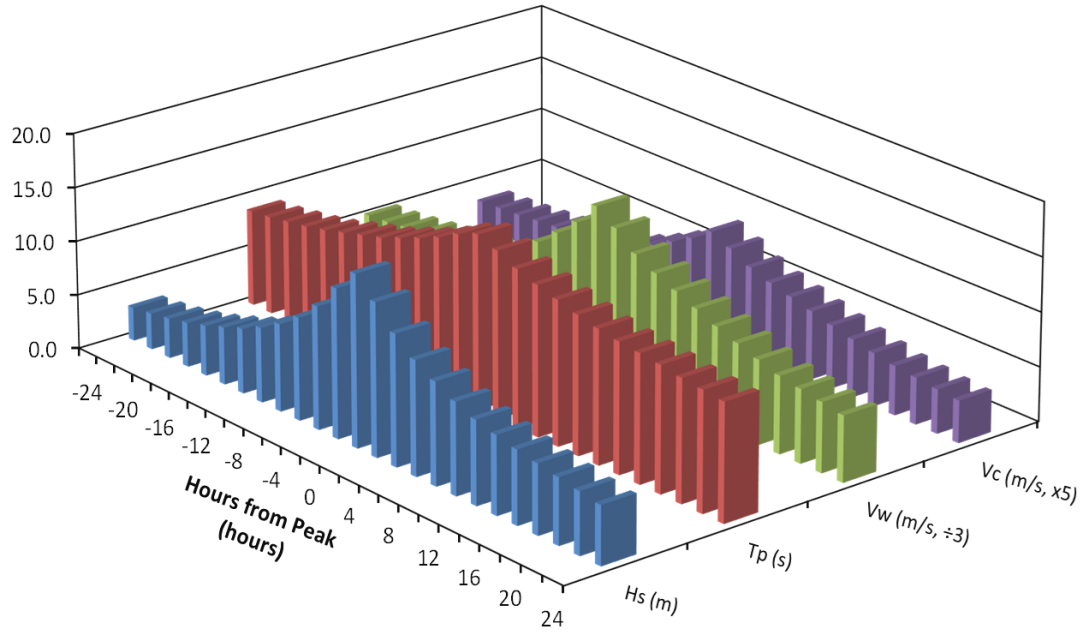

Fig. 10 Single event 100-year Hurricane 48 hours of ramping-up, reaching peak and ramping-down

Table 6 Single event - 100-year loop currents

Bin #	Hours from peak	Current speed (m/s)	Bin #	Hours from peak	Current speed (m/s)	Bin #	Hours from peak	Current speed (m/s)
1	-126	0.880	16	-36	2.228	31	54	1.953
2	-120	0.963	17	-30	2.310	32	60	1.870
3	-114	1.045	18	-24	2.393	33	66	1.760
4	-108	1.155	19	-18	2.475	34	72	1.678
5	-102	1.238	20	-12	2.585	35	78	1.595
6	-96	1.320	21	-6	2.668	36	84	1.513
7	-90	1.403	22	0	2.750	37	90	1.403
8	-84	1.513	23	6	2.668	38	96	1.320
9	-78	1.595	24	12	2.585	39	102	1.238
10	-72	1.678	25	18	2.475	40	108	1.155
11	-66	1.760	26	24	2.393	41	114	1.045
12	-60	1.870	27	30	2.310	42	120	0.963
13	-54	1.953	28	36	2.228	43	126	0.880
14	-48	2.035	29	42	2.118			
15	-42	2.118	30	48	2.035			

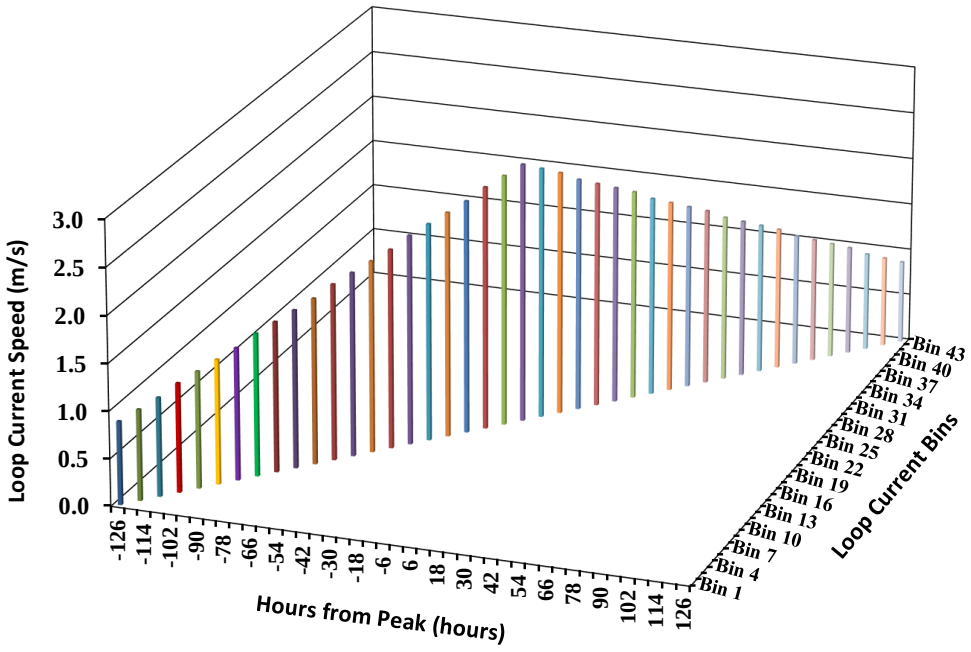

(a)

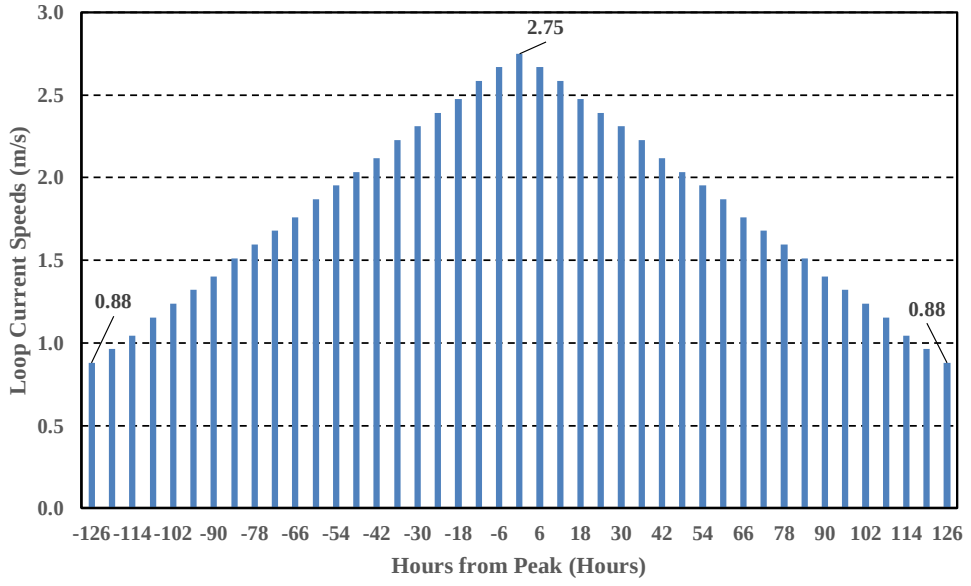

(b)

Fig. 11 (a) Single event 100-year loop current 252 hours of ramping-up, reaching peak and ramping-down and definition of loop current bins (b) Single event 100-year loop current 252 hours of ramping-up, reaching peak and ramping-down

Table 7 Loop Current Profile and Associated Wind and Waves

Wind Speed (10m elevation)	
1 h mean (m/s)	7.60
Waves	
Significant wave height (m)	2.00
Peak spectral period (s)	6.00
Normalized current profile	
Depth below surface (m)	Scale
0	1.00
50	0.99
150	0.66
300	0.35
600	0.20
1000+	0.20 m/s

5. Numerical models

5.1 Overview

A frequency-domain radiation/diffraction analysis panel model of the semisubmersible hull was developed to calculate added mass, potential damping, and motion Response Amplitude Operators (RAOs), serving as inputs for the subsequent time-domain analysis. The mooring fatigue analysis utilized a time-domain coupled approach. This section summarizes the numerical modeling considerations for environmental conditions, the diffraction panel model, moorings, risers, and other critical factors.

5.2 Environmental condition representation

5.2.1 Wind numerical models

Numerical models for wind were developed to accurately calculate mean wind forces at the combined hull and topsides wind center of pressure. Wind speeds were modeled to align with specified environmental parameters, and wind spectra were tailored according to API RP 2MET (2021). For hurricane winds, the ESDU wind spectrum was utilized, while ISO wind spectrum was applied for fatigue sea states as per the wave scatter diagram. The wind speed time series was generated using a sufficient number of harmonic components to avoid repetition throughout simulations.

5.2.2 Wave numerical models

Irregular wave series were generated by superimposing sinusoidal regular waves with varying heights, periods, and random phases for time-domain coupled analysis. Energy densities of the irregular wave series were carefully defined to encompass all wave frequencies, including low and high-frequency responses. The number of wave components used in each wave spectrum ensured that no part of the irregular wave series repeated during simulations.

API RP 2MET provided wave parameters such as significant wave height (Hs), peak period (Tp), maximum wave height (Hmax), and maximum wave crest height (Hc). Statistical analysis of these parameters for the generated wave time series was conducted to ensure they met acceptance criteria of +/-3% with respect to target values. If a generated wave train did not meet these criteria, it was discarded, and the generation process repeated until all acceptance criteria were satisfied. Only wave candidates meeting the correct key parameters were selected for numerical simulations.

5.2.3 Current numerical models

Current profiles ranging from the water surface to the seabed, as specified in API RP 2MET (2021), were modeled to match the described metocean criteria. The current loads on the platform hull, including drag coefficients on columns and pontoons, as well as shielding factors, were derived from wind tunnel underwater tests. Additionally, current drag loads on mooring lines and risers were simulated using a time-domain coupled program.

5.3 Deep draft semisubmersible platform

5.3.1 Platform mass properties

The platform's mass properties were accurately modeled using a weight management report that detailed component weight estimates for specific load cases outlined in the analysis matrix. Mass moments of inertia, or radii of gyration, were calculated based on detailed data for major platform components including topsides, primary hull structures, external appurtenances, and ballasts.

5.3.2 Hull diffraction/radiation model

A three-dimensional diffraction/radiation panel model was created to simulate the submerged platform hull. Panel sizes were adjusted in the wave zone to precisely compute low-frequency wave drift forces and moments. Different mesh sizes were generated, and hydrodynamic coefficients—such as added mass, low-frequency drift forces, and kinematics—were compared. The mesh size was fine-tuned until results such as added mass, drift forces, and velocity potentials converged and remained consistent across models. As the platform features spread moorings and is a semisubmersible, second-order difference-frequency excitations were computed using commercial software and integrated into the simulation.

5.3.3 Hull Morrison element model

To compensate for the lack of viscous effects in the hull diffraction/radiation model, Morrison elements were introduced, consisting of four columns and four pontoons. These Morrison elements of four columns were positioned to encompass each column entirely, covering both the submerged section and the freeboard. Drag coefficients for the four columns and four pontoons, relative to the incident wave heading, were typically derived from wind tunnel underwater tests. This approach was necessary because accurately calculating shielding effects for down-wave components proves challenging.

5.3.4 The combined diffraction/radiation and Morrison model

The comprehensive coupled dynamic analysis methodology highlighted in Zou (2008) is reproduced herein for ease of discussion and explanation. The general six-degrees-of-freedom (6-DOF) coupled dynamic equation of motion is expressed as follows

$$[\mathbf{M}]\{\ddot{\mathbf{U}}\}+[\mathbf{B}]\{\dot{\mathbf{U}}\}+[\mathbf{K}]\{\Delta\mathbf{U}\}=\{\mathbf{F}\}+\{\mathbf{F}_{visc}\}+\{\mathbf{F}_{m}\} \tag{9}$$

In Eq. (9),

[**M**] = mass and inertia matrix (6x6), hull structural mass and inertia + hull added mass and inertia + mass and added mass of slender members,

[**B**] = damping matrix (6x6), potential damping + viscous damping + wave drift damping on hull + damping of slender members + friction damping at riser keel guide frame,

[**K**] = stiffness matrix (6x6), hull hydrostatic stiffness (heave and roll/pitch) + stiffness due to moorings and risers,

{**F**}= load vector (6x1) of first- & second-order wave loads + wind loads, and/or other applied loads,

$\{\mathbf{F}_{visc}\}$= viscous loads (hull Morrison elements),

$\{\boldsymbol{F}_m\}$ = load vector (6x1) of mooring and riser tensions at the connected locations,

{**U** }= unknown motion vector (6x1) in the sequence of surge, sway, heave, roll, pitch, and yaw, respectively

Between the semi-submersible hull and moorings and risers, the instantaneously generated stiffness matrix [**K**], damping matrix [**C**], and load matrix $\{\boldsymbol{F}_m\}$ are exchanged back and forth during simulations. The detailed method and procedure inclusive of viscous effects have been described and presented in Das and Zou (2015).

5.4 Mooring lines and steel catenary risers (SCRs)

5.4.1 Mooring lines

Except for OPB/IPB analysis, individual chain links do not need to be modeled separately. Mooring lines have been modeled as finite elements based on segment geometry, length, unit dry/wet weight, and axial stiffness. Mooring line tensions, geometry, loads at fairleads and anchors, length of line on the seafloor, etc., are computed at each time step. Mooring drag/damping effects are considered simultaneously.

According to the ABS guide note (2021), two stiffness models for polyester, namely the upper and lower bound modulus methods, are acceptable. For non-loop current cases, static and dynamic stiffnesses are assumed to be 10MBL and 30MBL, respectively. In loop current cases, such as for VIM analysis, polyester stiffness is assumed to be 20MBL.

For OPB/IPB analysis, as shown in Fig. 1, the OVT components (main housing, latch housing, vertical pin diameter, horizontal pin diameter, and corresponding friction coefficients from the vendor) and a few top individual chain links (e.g., top 3 links) have been modeled. Additionally, one equivalent element represents the remaining chain links (e.g., chain links 4 to 20), following BV Guidelines (2014). While BV recommends modeling individual top 20 chain links for OPB/IPB analysis, our experience suggests that modeling all 20 links individually is excessive and unnecessary. However, the effects of the remaining top chain links, such as equivalent mass, stiffness, and damping, are accounted for and represented by this equivalent element. Further discussions on these findings will be presented in Section 7: Numerical analysis results.

5.4.2 Steel catenary risers (SCRs)

SCRs have been modeled as finite elements, considering segment geometry, length, unit dry/wet weight, axial stiffness, hydrodynamic drag, and added mass coefficients. Additionally, SCRs have been equipped with external strakes along their length, aimed at mitigating Vortex-Induced Vibration (VIV) effects from the top down to approximately 50% of their suspended length in the

water column. The contributions of these strakes to current loads and damping have been incorporated into the simulations.

5.5 Vortex induced motion (VIM) responses

With over two decades of measured data, including extensive model testing and field measurements, prescribed Max A/D and Normal A/D curves as a function of reduced velocities will be utilized.

For a given current bin in a specified heading, the platform's transverse period and corresponding reduced velocity can be calculated. VIM motion amplitudes, either Maximum or Normal, are computed based on the Max A/D or Normal A/D curves corresponding to the specified heading.

According to DNV RP F205 (2021), since vortex shedding follows a sinusoidal process, it is appropriate to model the crossflow force acting on the hull as harmonic in time at the shedding frequency. It is important to note that the amplitude of the imposed crossflow force should be iteratively adjusted to ensure that the transverse motion amplitude meets the prescribed value from the VIM analysis curves.

An alternative approach is to apply the imposed platform transverse motion amplitude directly at the shedding frequency. It is recommended to verify that the imposed transverse motion amplitude satisfies the specified value through double-checking.

The set of VIM curves incorporating appropriate damping contributions from moorings and risers has been utilized in this study to mitigate traditional over-conservative assumptions. Ma *et al*. (2013) conducted full-scale VIM field measurements on a semi-submersible and found that the actual severity and persistence of VIM are significantly lower than those observed in VIM model tests. They attributed these differences to discrepancies between the model scale and real-world conditions.

Zou *et al*. (2014) highlighted another significant factor, noting that VIM tests often omit damping contributions from moorings and SCRs. They found that the measured damping due to the platform hull in tests is about 1/5 to 1/4 of the prototype damping when moorings and risers are present in corresponding loop currents. VIM motion is a resonant low-frequency response that is highly sensitive to system damping. An unrealistically lightly damped system can lead to unrealistically high VIM resonant responses.

In practical field conditions, observed platform VIM motion amplitudes are notably lower than those derived in laboratory tests. Sterenborg *et al*. (2016) were the first to introduce an active damping device for VIM tests, aiming to simulate damping contributions from moorings and risers in a controlled manner.

6. Key input data for analysis

6.1 Overview

There are some key input data for VIM induced fatigue analysis and OPB/IP fatigue analysis undertaken for this study and highlighted in this section.

6.2 Prescribed VIM curves

VIM nominal transverse A/D, nominal in-line A/D, and nominal Yaw angle design envelope curves as a function of reduced velocities are employed to calculate forced vessel motions. Nominal

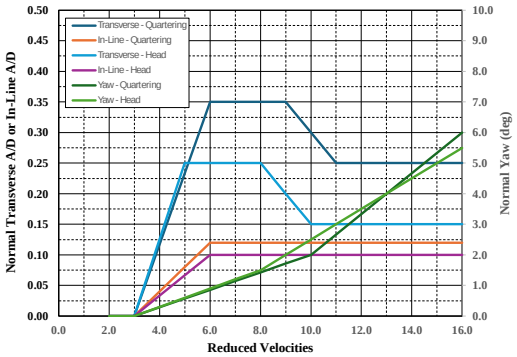

(a) Prescribed normal VIM curves

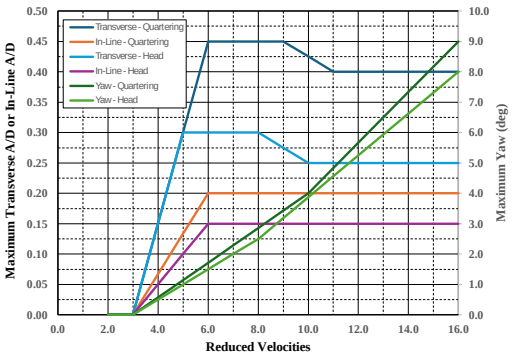

(b) Prescribed max VIM curves

Fig. 12 Prescribed normal and max VIM curves

Table 8 Prescribed VIM Curves

Reduced Velocities	Quartering Directions						Head Directions					
	Transverse		In-Line		Yaw		Transverse		In-Line		Yaw	
	Normal	Max	Normal	Max	Normal	Max	Normal	Max	Normal	Max	Normal	Max
3.0	0.000	0.000	0.000	0.000	0.000	0.000	0.000	0.000	0.000	0.000	0.000	0.000
5.0	0.233	0.300	0.080	0.133	0.571	1.143	0.250	0.300	0.067	0.100	0.600	1.000
6.0	0.350	0.450	0.120	0.200	0.857	1.714	0.250	0.300	0.100	0.150	0.900	1.500
7.0	0.350	0.450	0.120	0.200	1.143	2.286	0.250	0.300	0.100	0.150	1.200	2.000
8.0	0.350	0.450	0.120	0.200	1.429	2.857	0.250	0.300	0.100	0.150	1.500	2.500
9.0	0.350	0.450	0.120	0.200	1.714	3.429	0.200	0.275	0.100	0.150	2.000	3.188
10.0	0.300	0.425	0.120	0.200	2.000	4.000	0.150	0.250	0.100	0.150	2.500	3.875
11.0	0.250	0.400	0.120	0.200	2.667	4.833	0.150	0.250	0.100	0.150	3.000	4.563
14.0	0.250	0.400	0.120	0.200	4.667	7.333	0.150	0.250	0.100	0.150	4.500	6.625
16.0	0.250	0.400	0.120	0.200	6.000	9.000	0.150	0.250	0.100	0.150	5.500	8.000

transverse A/D or nominal in-line A/D is defined as: RMS (A) * $\sqrt{2}$/D, "A" stands the amplitudes of VIM motions either transverse or in-line and "D" is the characteristic length of the column. Nominal yaw angle is defined as: RMS (Yaw) *$\sqrt{2}$, "Yaw" represents the amplitudes of VIM indued yaw motions.

All prescribed VIM curves in this study are derived from model test results of previous similar projects, incorporating active damping contributions from moorings and risers. It is assumed for this analysis that fatigue damage calculations, which are proportional to stresses or tensions raised to the power of three, may be slightly conservative when using nominal A/D curves. However, calculations using maximum A/D curves are deemed excessively conservative and are not recommended for mooring design purposes.

The prescribed VIM curves of nominal and maximum transverse A/D, nominal and maximum in-line A/D and nominal and maximum yaws are summarized in Table 8 and illustrated in Fig. 12.

6.3 Coefficients of slender elements

The drag (Cd) and added mass (Ca) coefficients of the chain, polyester rope, bare riser and straked risers for analysis are highlighted as follows,

- Chain: Cd=2.4, Ca=1.0
- Polyester rope: Cd=1.6, Ca=1.0
- Bare riser: Cd=1.0, Ca=1.0
- Straked risers: Cd=2.0, Ca=2.0

6.4 Corrosion allowances

A corrosion allowance of 0.3 mm/year has been incorporated into the sizing of both upper and lower chains. Hydrodynamic effects and weights are calculated based on the non-corroded dimensions. For mooring line fatigue analysis, 50% of the chain corrosion allowance has been considered.

6.5 Friction coefficients and breakout angles

The friction coefficients of both vertical and horizontal pins and OPB and IPB breakout angles for this study are summarized as follows,

- Friction coefficient: 0.07
- OPB breakout angle: 0.2 deg
- IPB breakout angle: 0.6 deg

7. Numerical analysis results

7.1 Overview

Numerical analysis results for tension-tension (TT) fatigue are presented in Sections 7.2 to 7.5, covering:

a) Wave scatter diagram effects
b) Current distribution bins impact
c) Single events (100-year hurricanes and loop currents)
d) Combined effects of OPB/IPB/TT fatigue

7.2 TT fatigues – wave scatter diagram

The wave scatter diagram is detailed in Section 4.2, while API TN and DNV SN curves are discussed in Sections 2.1.1 and 2.1.2, respectively. TT fatigue analysis results are summarized in Tables 9(a) and 9(b), and illustrated in Fig. 12. The platform's design service life is 25 years with a minimum safety factor of 10, resulting in a required minimum fatigue life of 250 years.

Table 9a TT Fatigues (ML#1 to ML#8) – Wave Scatter Diagram: DNV SN Curve vs API TN Curve

	ML1	ML2	ML3	ML4	ML5	ML6	ML7	ML8
	Years	Years	Years	Years	Years	Years	Years	Years
DNV SN curve	26,438	25,942	25,004	24,560	22,805	23,193	24,009	24,439
API TN curve	10,618	10,418	10,042	9,864	9,159	9,314	9,642	9,815

Table 9b TT Fatigues (ML#9 to ML#16) – Wave Scatter Diagram: DNV SN Curve vs API TN Curve

	ML9	ML10	ML11	ML12	ML13	ML14	ML15	ML16
	Years	Years	Years	Years	Years	Years	Years	Years
DNV SN curve	25,753	26,422	27,869	28,654	26,314	25,623	24,344	23,752
API TN curve	10,343	10,611	11,193	11,508	10,568	10,290	9,777	9,539

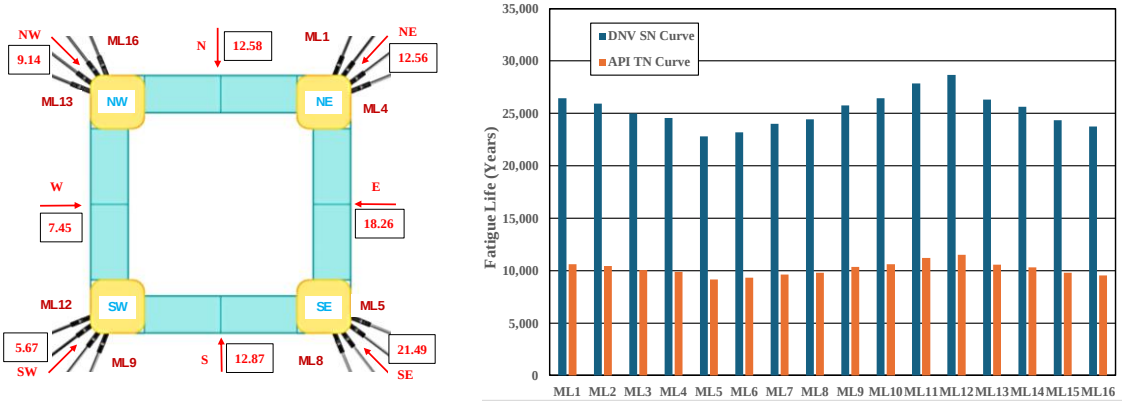

(a) Wave probability distributions (b) TT fatigue life, SN curve vs TN curve

Fig. 13 Wave probability distributions and TT fatigue life, SN curve vs TN curve

In Fig. 13(a), values in black boxes denote wave probability distributions, with the highest probability observed from grid Southeast. Table 9a and 9b, along with Fig. 13, show that the lowest fatigue lives for mooring line #5 are 22,805 years and 9,159 years according to the DNV SN and API TN curves, respectively, both well exceeding the required minimum fatigue life.

7.3 TT fatigues – current distribution bins

Current distribution bins are detailed in Section 4.3, and the prescribed VIM curves are highlighted in Section 6.2. TT fatigue analysis results are summarized in Tables 10(a) and 10(b), and displayed in Fig. 13.

In Fig. 14(a), values in black boxes depict current bin probability distributions, with the highest probability observed from grid Southwest. Tables 10(a) and 10(b), along with Fig. 14, show that the

Table 10a TT Fatigues (ML#1 to ML#8) – Wave Scatter Diagram: DNV SN Curve vs API TN Curve

	ML1	ML2	ML3	ML4	ML5	ML6	ML7	ML8
	Years	Years	Years	Years	Years	Years	Years	Years
DNV SN curve	4,180	4,337	4,506	4,566	1,750	1,815	1,886	1,911
API TN curve	1,679	1,742	1,810	1,834	703	729	758	768

Table 10b TT Fatigues (ML#9 to ML#16) – Wave Scatter Diagram: DNV SN Curve vs API TN Curve

	ML9	ML10	ML11	ML12	ML13	ML14	ML15	ML16
	Years	Years	Years	Years	Years	Years	Years	Years
DNV SN curve	3,512	3,466	3,336	3,215	2,058	2,136	2,219	2,248
API TN curve	1,411	1,392	1,340	1,291	827	858	891	903

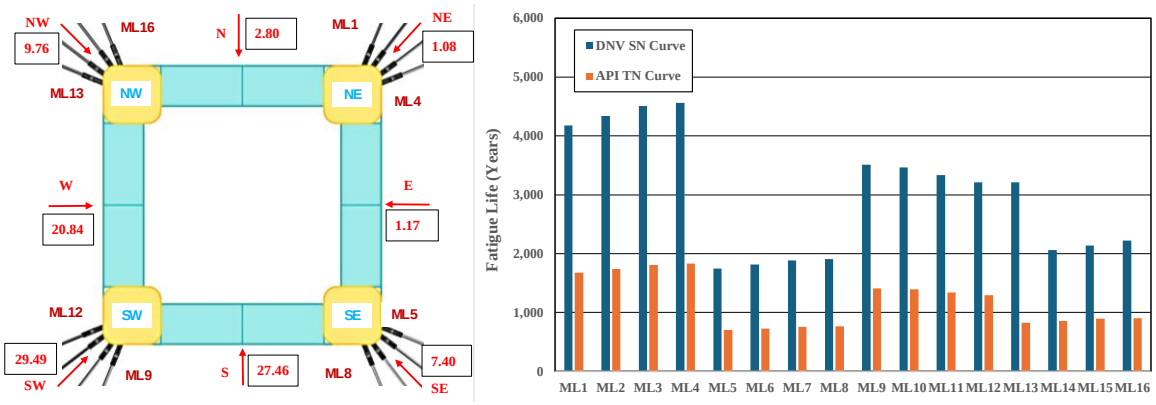

(a) Current probability distributions (b) TT fatigue life, SN curve vs TN curve

Fig. 14 Current probability distributions and TT fatigue life, SN curve vs TN curve

lowest fatigue lives for mooring line #5 are 1,750 years and 703 years according to the DNV SN and API TN curves, respectively, both above the required minimum fatigue life.

Comparing Tables 9(a), 9(b), 10(a), and 10(b), TT fatigues due to VIM motions are significantly more severe than those due to waves.

7.4 TT fatigues – single events

Single event fatigue assessments were conducted to validate the robustness of the proposed mooring design under 100-year hurricanes and 100-year loop currents, as outlined in API RP 2T (2010). The criteria include ensuring that the calculated damage from each single extreme event does not exceed 10% of the allowable long-term fatigue damage and prohibiting the combination of single event damage with long-term fatigue damage.

Table 11a TT Fatigue Damages (ML#1 to ML#8) – 100-year Hurricanes: DNV SN Curve vs API TN Curve

	ML1	ML2	ML3	ML4	ML5	ML6	ML7	ML8
	1/year	1/year	1/year	1/year	1/year	1/year	1/year	1/year
DNV SN curve	8.2E-05	6.8E-05	5.7E-05	4.8E-05	6.9E-04	8.2E-04	9.8E-04	1.2E-03
API TN curve	2.0E-04	1.7E-04	1.4E-04	1.2E-04	1.7E-03	2.0E-03	2.4E-03	2.9E-03
Max allowed damage	1.0E-02	1.0E-02	1.0E-02	1.0E-02	1.0E-02	1.0E-02	1.0E-02	1.0E-02
Meet design criteria?	Yes	Yes	Yes	Yes	Yes	Yes	Yes	Yes

Table 11b TT Fatigue Damages (ML#9 to ML#16) – 100-year Hurricanes: DNV SN Curve vs API TN Curve

	ML9	ML10	ML11	ML12	ML13	ML14	ML15	ML16
	1/year	1/year	1/year	1/year	1/year	1/year	1/year	1/year
DNV SN curve	9.3E-05	7.8E-05	6.6E-05	5.5E-05	1.2E-04	1.5E-04	1.8E-04	2.1E-04
API TN curve	2.3E-04	1.9E-04	1.6E-04	1.4E-04	3.1E-04	3.7E-04	4.4E-04	5.2E-04
Max allowed damage	1.0E-02	1.0E-02	1.0E-02	1.0E-02	1.0E-02	1.0E-02	1.0E-02	1.0E-02
Meet design criteria?	Yes	Yes	Yes	Yes	Yes	Yes	Yes	Yes

Each single extreme event involves ramping-up, reaching peak, and ramping-down phases, as detailed in Sections 4.4 and 4.5. Fatigue damage is calculated for each time interval of the event and then aggregated. The analysis primarily considered the worst heading:

- For 100-year hurricanes, the wave heading assumed was from the Grid Southeast.
- For 100-year loop currents, the current direction analyzed was from the Grid Southwest.

7.4.1 TT fatigues – 100-year hurricanes

The single event of a 100-year hurricane, lasting 48 hours and encompassing associated winds and currents, is detailed in Section 4.4. The fatigue damage results for TT (tension-tension) are presented in Tables 11(a) and 11(b) and illustrated in Fig. 15.

According to Section 2.1.4, the minimum safety factor for TT fatigue is 10, and the calculated damage from each event must not exceed 10% of the allowable long-term fatigue damage. In Fig. 15(a), the red horizontal line signifies the maximum allowable fatigue damage (1.0E-02).

From Fig. 15(a), it is evident that the highest fatigue damages for mooring line #8 are 1.2E-3 and 2.9E-3 per DNV SN curve and API TN curve, respectively, both of which fall below the maximum allowable fatigue damage threshold. The breakdown of fatigue damages for mooring line #8 is depicted in Fig. 14(b), highlighting that the fatigue damage from Bin 13 (representing peak waves/winds/currents, see Table 5) predominates and governs the overall fatigue assessment.

7.4.2 TT fatigues – 100-year loop currents

The single event of a 100-year loop current, lasting 252 hours and including associated winds and waves, is detailed in Section 4.5. TT fatigue damage results based on normal VIM curves are summarized in Tables 12(a) and 12(b) and illustrated in Fig. 16, while TT fatigue damage results based on maximum VIM curves are given in Tables 13(a) and 13(b) and presented in Fig. 16.

Table 12a TT Fatigue Damages (ML#1 to ML#8), Normal VIM Curves, 100-year Loop Currents: DNV SN Curve vs API TN Curve

	ML1	ML2	ML3	ML4	ML5	ML6	ML7	ML8
	1/year	1/year	1/year	1/year	1/year	1/year	1/year	1/year
DNV SN curve	2.28E-04	2.18E-04	2.08E-04	1.99E-04	1.81E-03	2.02E-03	2.23E-03	2.43E-03
API TN curve	5.67E-04	5.43E-04	5.19E-04	4.94E-04	4.51E-03	5.03E-03	5.54E-03	6.06E-03
Max allowed damage	1.0E-02	1.0E-02	1.0E-02	1.0E-02	1.0E-02	1.0E-02	1.0E-02	1.0E-02
Meet design criteria?	Yes	Yes	Yes	Yes	Yes	Yes	Yes	Yes

Table 12b TT Fatigue Damages (ML#9 to ML#16), Normal VIM Curves, – 100-year Loop Currents: DNV SN Curve vs API TN Curve

	ML9	ML10	ML11	ML12	ML13	ML14	ML15	ML16
	1/year	1/year	1/year	1/year	1/year	1/year	1/year	1/year
DNV SN curve	2.86E-04	3.22E-04	3.59E-04	3.95E-04	2.06E-03	1.96E-03	1.86E-03	1.76E-03
API TN curve	7.12E-04	8.03E-04	8.94E-04	9.84E-04	5.12E-03	4.88E-03	4.63E-03	4.39E-03
Max allowed damage	1.0E-02	1.0E-02	1.0E-02	1.0E-02	1.0E-02	1.0E-02	1.0E-02	1.0E-02
Meet design criteria?	Yes	Yes	Yes	Yes	Yes	Yes	Yes	Yes

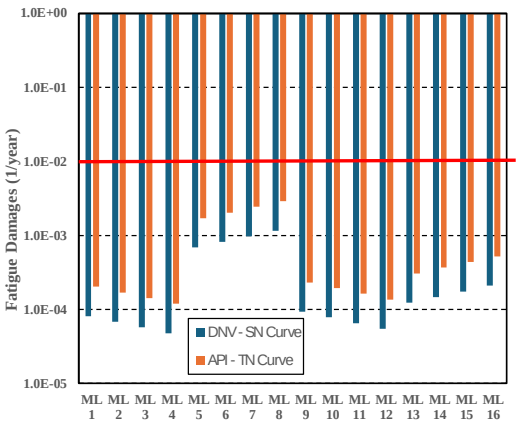

(a) TT fatigue damages – 100-year hurricanes, SN curve vs TN curve

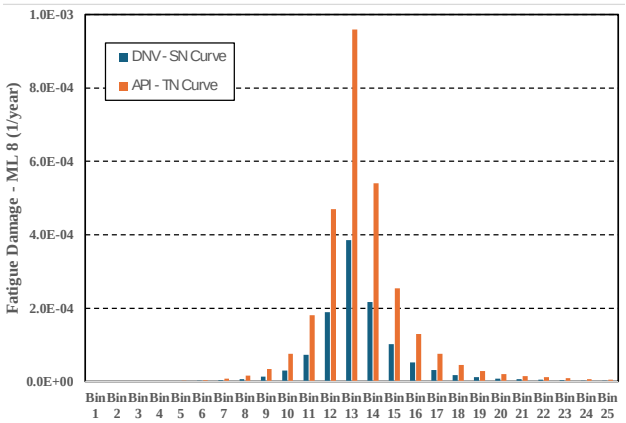

(b) TT fatigue damage breakdowns of ML 8 - 100-year hurricanes, SN curve vs TN curve

Fig. 15 TT fatigue damages in 100-year hurricanes and TT fatigue damage breakdowns of ML 8 SN curve vs TN curve

As elaborated in Section 7.4.1, the red horizontal line shown in Fig. 15(a) represents the maximum allowable fatigue damage (1.0E-02). From Tables 12(a) and 12(b), it is observed that the highest fatigue damages of mooring line #8 are 2.43E-3 and 6.06E-3 per DNV SN curve and API

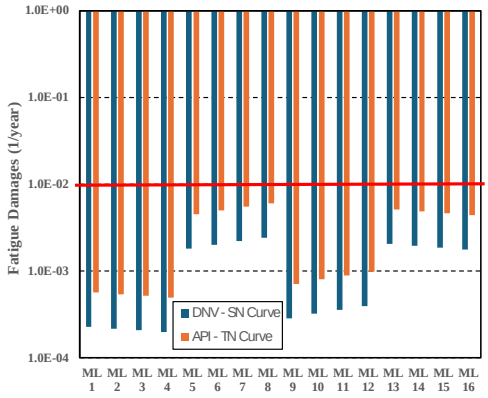

(a) TT fatigue damages, normal VIM curves, 100-year loop currents, SN curve vs TN curve

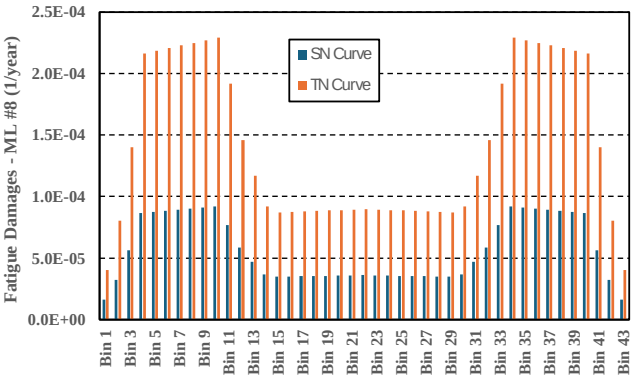

(b) TT fatigue damage breakdowns of ML 8, normal VIM curves, 100-year loop currents, SN curve vs TN curve

Fig. 16 TT fatigue damages in 100-year loop currents, Normal VIM curves and TT fatigue damage breakdowns of ML 8, SN curve vs TN curve

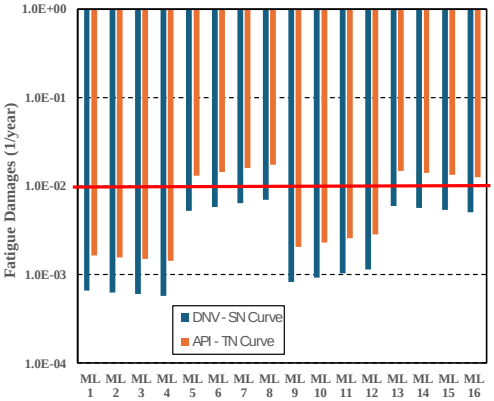

(a) TT fatigue damages, max VIM curves, 100-year loop currents, SN curve vs TN curve

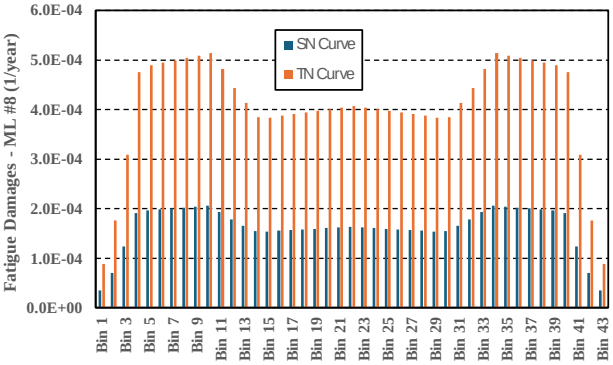

(b) TT fatigue damage breakdowns of ML 8, max VIM curves, 100-year loop currents, SN curve vs TN curve

Fig. 17 TT fatigue damages in 100-year loop currents, max VIM curves and TT fatigue damage breakdowns of ML 8, SN curve vs TN curve

TN curve, respectively, both of which are below the maximum allowable fatigue damage. The breakdowns of fatigue damages for mooring line #8 are shown in Fig. 16(b), where the fatigue damages from Bin 10 and Bin 34 (as defined in Table 6) are the highest. It is noted that the highest fatigue damage bin does not correlate with the highest current speed due to its reduced velocity being outside the lock-in region.

From Tables 13(a) and 13(b), the highest fatigue damage of mooring line #8 is 7.03E-3 per DNV SN curve, which is also below the maximum allowable fatigue damage. However, mooring lines #5 to #8 and #13 to #16 all exhibit fatigue damages above the maximum allowable per API TN curve, failing to meet the requirement. Breakdowns of the highest fatigue damage for mooring line #8 are shown in Fig. 17(b).

Table 13a TT Fatigue Damages (ML#1 to ML#8), Max VIM Curves, 100-year Loop Currents: DNV SN Curve vs API TN Curve

	ML1	ML2	ML3	ML4	ML5	ML6	ML7	ML8
	1/year	1/year	1/year	1/year	1/year	1/year	1/year	1/year
DNV SN curve	6.58E-04	6.30E-04	6.01E-04	5.73E-04	5.23E-03	5.83E-03	6.43E-03	7.03E-03
Max allowed damage	1.0E-02	1.0E-02	1.0E-02	1.0E-02	1.0E-02	1.0E-02	1.0E-02	1.0E-02
Meet design criteria?	Yes	Yes	Yes	Yes	Yes	Yes	Yes	Yes
API TN curve	1.64E-03	1.57E-03	1.50E-03	1.43E-03	1.30E-02	1.45E-02	1.60E-02	1.75E-02
Meet design criteria?	Yes	Yes	Yes	Yes	No	No	No	No

Table 13b TT Fatigue Damages (ML#9 to ML#16), Max VIM Curves, – 100-year Loop Currents: DNV SN Curve vs API TN Curve

	ML9	ML10	ML11	ML12	ML13	ML14	ML15	ML16
	1/year	1/year	1/year	1/year	1/year	1/year	1/year	1/year
DNV SN curve	8.26E-04	9.31E-04	1.04E-03	1.14E-03	5.94E-03	5.66E-03	5.38E-03	5.09E-03
Max allowed damage	1.0E-02	1.0E-02	1.0E-02	1.0E-02	1.0E-02	1.0E-02	1.0E-02	1.0E-02
Meet design criteria?	Yes	Yes	Yes	Yes	Yes	Yes	Yes	Yes
API TN curve	2.06E-03	2.32E-03	2.58E-03	2.84E-03	1.48E-02	1.41E-02	1.34E-02	1.27E-02
Meet design criteria?	Yes	Yes	Yes	Yes	No	No	No	No

Further discussions regarding mooring fatigue damages from the single event of a 100-year loop current are highlighted in Section 8 Discussions.

7.5 OPB/IPB/TT combined fatigue

7.5.1 OPB/IPB moments at chain links #1 and #3

According to BV Guidelines (2014), it is recommended to model the top 20 chain links individually. However, for practicality, modeling the top three chain links individually is deemed sufficient, while the remaining 17 chain links can be represented by a single equivalent element. This approach is applied to mooring line #5 for a specific fatigue bin from Southeast, where Hs=2.75 m, Tp=8.0 sec, and the corresponding probability is 0.746%.

Figs. 18 and 19 illustrate segments of the time series of OPB/IPB moments at Chain Links #1 and #3, respectively. The standard deviations of OPB/IPB moments at Chain Link #1 are approximately 5.1 and 6.3 times larger than those at Chain Link #3.

From Fig. 18, it is evident that OPB moments remain "flat and constant" between approximately 3,100 sec to 3,150 sec and from 3,250 sec to 3,270 sec. This suggests that the horizontal pin connecting the latch housing and main housing (as shown in Fig. 1) reaches the sliding moment limit (Eq. (5)).

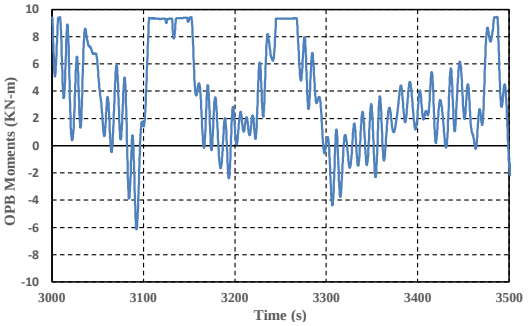

(a) Sample time series of OPB moments at chain links #1 (Hs=2.75 m, Tp=8.0s)

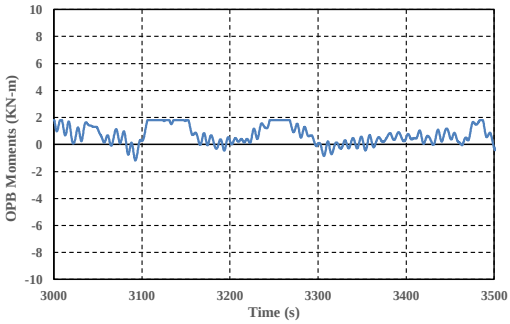

(b) Sample time series of OPB moments at chain links #3 (Hs=2.75 m, Tp=8.0 s)

Fig. 18 Sample time series of OPB moments at chain links #1 and #3

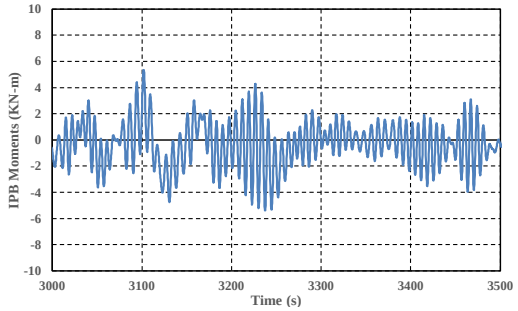

(a) Sample time series of IPB moments at chain links #1 (Hs=2.75 m, Tp=8.0s)

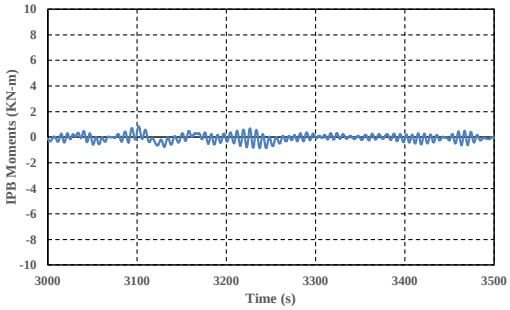

(b) Sample time series of IPB moments at chain links #3 (Hs=2.75 m, Tp=8.0 s)

Fig. 19 Sample time series of IPB moments at chain links #1 and #3

In contrast, Fig. 19 depicts IPB moments with different response characteristics, showing relatively frequent oscillations without any "flat and constant" instances. This indicates that the vertical pin connecting the main housing and OVT foundation (Fig. 1) does not reach the sliding moment limit.

7.5.2 6-DOF motion amplitude spectra at OVT #5

To explore the interconnected dynamics between the 6 degrees of freedom (DOF) motions at OVT #5 (Fig. 4) and OPB/IPB moments, amplitude spectra of the 6-DOF motions at OVT #5 have been generated and are presented in Fig. 20.

As stated in Section 5.4.1, polyester rope was utilized, and its stiffness characteristics vary significantly. The stiffness ranges from 10 times the minimum breaking load (MBL) for static installation to 20 MBL for loop currents mooring analysis, and up to 30 MBL for calculating extreme mooring line tension. These variations affect the natural periods of surge/sway and roll/pitch/yaw. Interestingly, heave natural period remains largely unaffected.

As an example, the platform natural periods with a stiffness of 20MBL have been given, Surge/Sway: 125 seconds; Heave: 22 seconds; Roll/Pitch: 35 seconds and Yaw: 65 seconds.

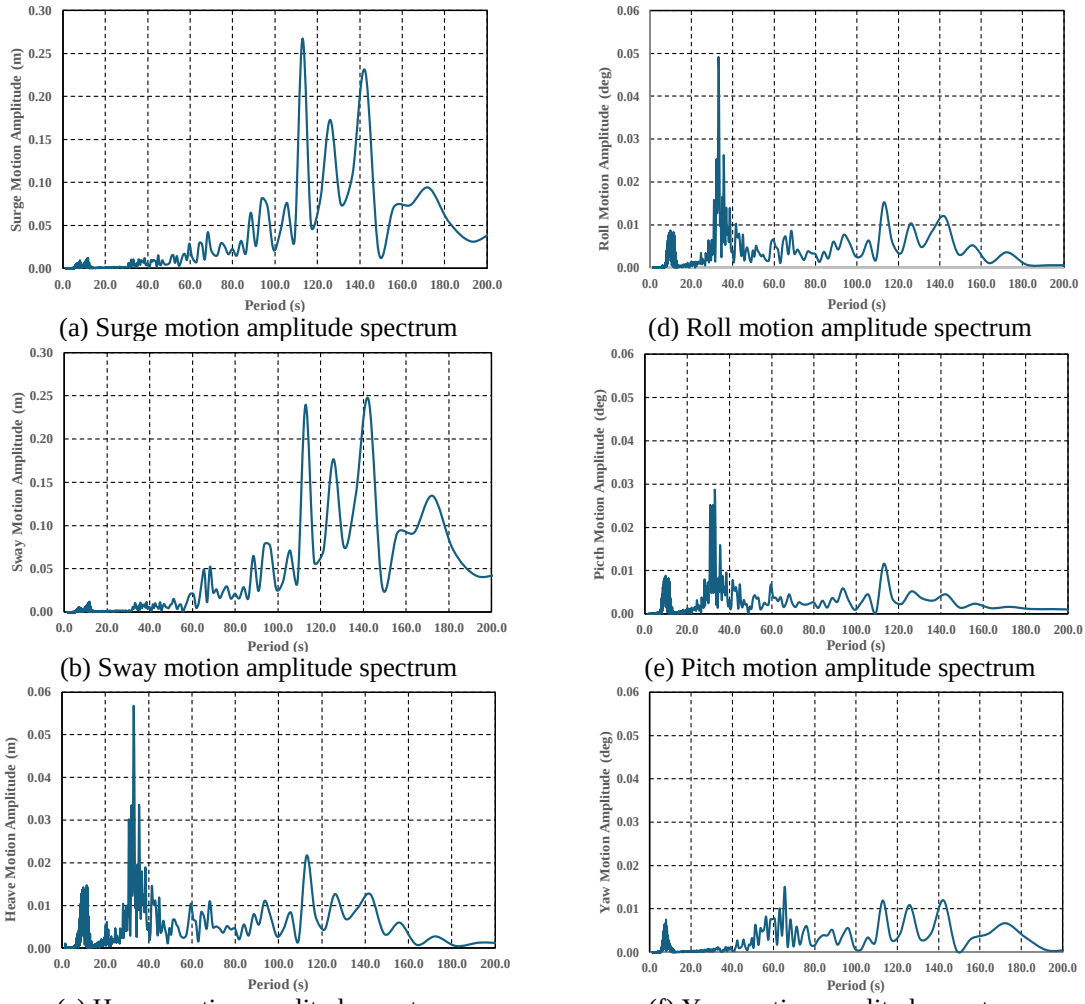

(a) Surge motion amplitude spectrum

(d) Roll motion amplitude spectrum

(b) Sway motion amplitude spectrum

(e) Pitch motion amplitude spectrum

(c) Heave motion amplitude spectrum

(f) Yaw motion amplitude spectrum

Fig. 20 6-DOF motion amplitude spectra at OVT #5

Surge and sway motions (Figs. 20(a) and 20(b)) are predominantly influenced by low-frequency components. Located away from the platform center, OVT #5 exhibits noticeable vertical motions induced by roll and pitch (Fig. 20(c)).

Variations in mooring line tensions are significantly influenced by surge and sway motions. Simultaneously, heave, roll, pitch, and yaw motions are affected by changes in mooring line tensions, primarily driven by surge and sway motions. These coupling effects are evident and captured in the analysis.

7.5.3 OPB/IPB moment amplitude spectra

To investigate the characteristics of OPB/IPB moments, amplitude spectra of OPB/IPB moments at chain link #1 of mooring line #5 have been generated and are illustrated in Fig. 21. Several observations are highlighted below:

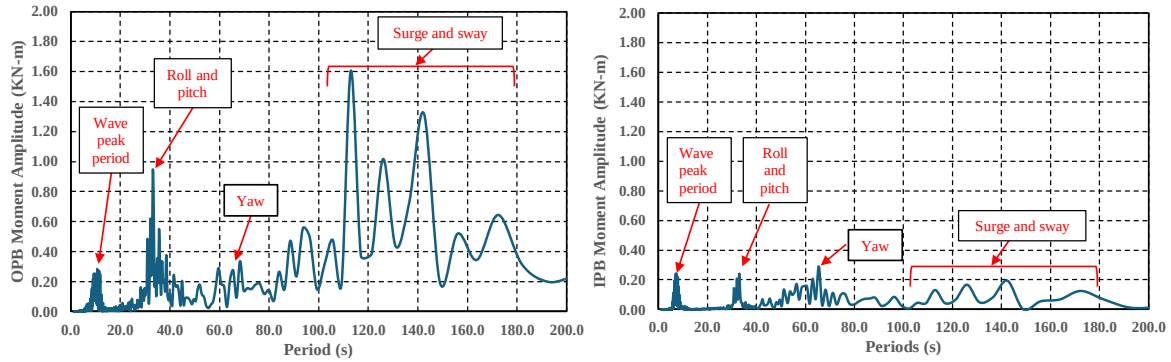

(a) OPB moment amplitude spectrum (b) IPB moment amplitude spectrum

Fig. 21 OPB and IPB moment amplitude spectra at chain links #1 of mooring line #5

- OPB moments exhibit significant low-frequency components induced by roll, pitch, yaw, and surge/sway, consistent with observations in Fig. 21(a).
- IPB moments show a similar distribution of wave frequency components due to incident wave energy, along with low-frequency components induced by yaw, as seen in Fig. 21(b). However, IPB moments contain noticeably fewer low-frequency components induced by roll, pitch, and surge/sway compared to Fig. 21(b).
- Both OPB and IPB moments at chain link #1 of mooring line #5 (Fig. 20) clearly demonstrate coupling with the 6-DOF motions at OVT #5 (Fig. 20).

7.5.4 Sample calculation of the combined stresses

In Section 2.2.3, the document describes hot spots A, B, B', and C, including their respective stress concentration factors. Section 2.2.4 presents the formula used to calculate combined stresses for the selected sample bin. This section also provides a step-by-step procedure for computing combined stresses at hot spots A, B, B', and C respectively.

At hot spot A

$$\Delta\sigma_{combined} = Z_{corr}(\Delta\sigma_{TT} + Z_s\Delta\sigma_{IPB}) \quad \text{-> A1}$$

$$\Delta\sigma_{combined} = Z_{corr}(\Delta\sigma_{TT} - Z_s\Delta\sigma_{IPB}) \quad \text{-> A2}$$

At hot spots B, B' and C

$$\Delta\sigma_{combined} = Z_{corr}(\Delta\sigma_{TT} + Z_S\Delta\sigma_{OPB} + Z_s\Delta\sigma_{IPB}) \quad \text{-> B1 or B1' or C1}$$

$$\Delta\sigma_{combined} = Z_{corr}(\Delta\sigma_{TT} + Z_S\Delta\sigma_{OPB} - Z_s\Delta\sigma_{IPB}) \quad \text{-> B2 or B2' or C2}$$

$$\Delta\sigma_{combined} = Z_{corr}(\Delta\sigma_{TT} - Z_S\Delta\sigma_{OPB} + Z_s\Delta\sigma_{IPB}) \quad \text{-> B3 or B3' or C3}$$

$$\Delta\sigma_{combined} = Z_{corr}(\Delta\sigma_{TT} - Z_S\Delta\sigma_{OPB} - Z_s\Delta\sigma_{IPB}) \quad \text{-> B4 or B4' or C4}$$

Time series of the factored combined stresses at hot spots A, B, B' and C have been plotted and displayed in Fig. 22 and corresponding standard deviations of these hot spots are summarized in Table 14.

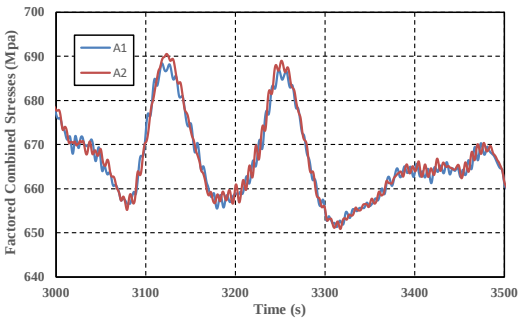

(a) Time series of the factored combined stressed at hot spot A

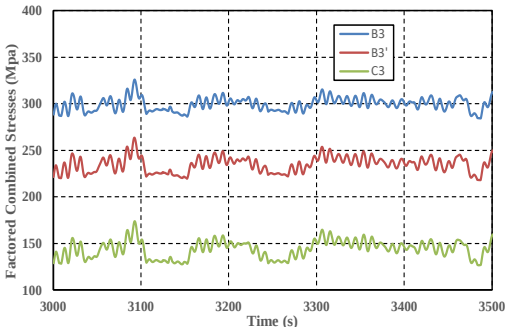

(d) Time series of the factored combined stressed at hot spots B3, B3’ and C3

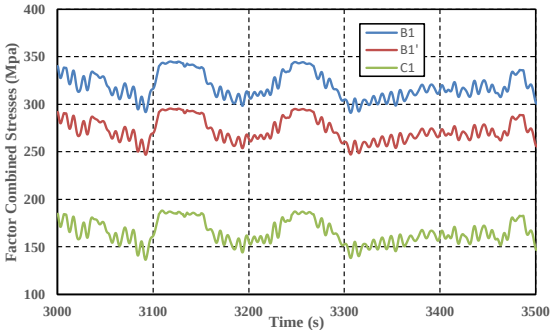

(b) Time series of the factored combined stressed at hot spots B1, B1’ and C1

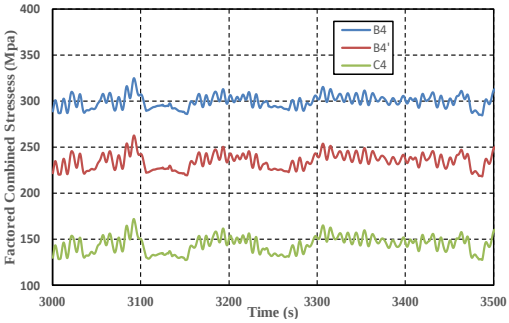

(e) Time series of the factored combined stressed at hot spots B4, B4’ and C4

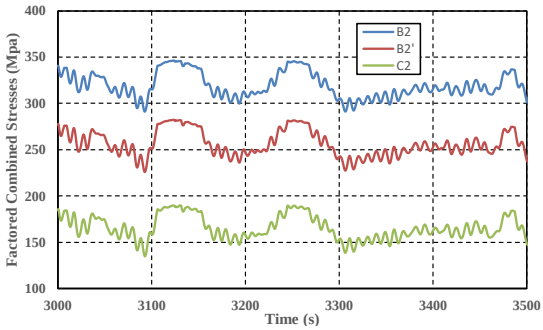

(c) Time series of the factored combined stressed at hot spots B2, B2’ and C2

Fig. 22 Time series of the combined stresses at hot spots A, B, B’ and C

Some observations from Fig. 22 are highlighted as follows,

- *Stress Magnitudes*: the magnitudes of factored combined stresses vary significantly at hot spots A, B, B’, and C, with the highest magnitudes occurring at hot spot A.
- *Response Characteristics*: the response characteristics of the factored stresses at hot spot A are notably different from those at hot spots B, B’, and C. Additionally, similar response characteristics are observed among B1, B1’, C1 (Fig. 22(b)) and B2, B2’, C2 (Fig. 22(c)), but these differ significantly from those at B3, B3’, C3 (Fig. 22(d)) and B4, B4’, C4 (Fig. 22(e)).

Table 14 Standard deviations of the factored combined stresses

Hot spots		standard deviations (Mpa)	% variation at same hot spot
A	A1	7.65	96%
	A2	7.94	100%
B	B1	12.07	99%
	B2	12.20	100%
	B3	6.79	56%
	B4	6.73	55%
B’	B1’	12.19	99%
	B2’	12.31	100%
	B3’	7.96	65%
	B4’	7.88	64%
C	C1	11.25	98%
	C2	11.50	100%
	C3	8.72	76%
	C4	8.52	74%

Table 15a OPB/IPB/TT Fatigues (ML#1 to ML#8), BV SN Curve for the Combined Stresses

	ML1	ML2	ML3	ML4	ML5	ML6	ML7	ML8
	years	years	years	years	years	years	years	years
BV SN curve	1,661	1,619	1,578	1,540	1,263	1,302	1,343	1,372
Min fatigue life	75	75	75	75	75	75	75	75
Meet design criteria?	Yes	Yes	Yes	Yes	Yes	Yes	Yes	Yes

Table 15b OPB/IPB/TT Fatigues (ML#9 to ML#16), BV SN Curve for the Combined Stresses

	ML9	ML10	ML11	ML12	ML13	ML14	ML15	ML16
	years	years	years	years	years	years	years	years
BV SN curve	1,568	1,608	1,650	1,695	1,427	1,460	1,494	1,530
Min fatigue life	75	75	75	75	75	75	75	75
Meet design criteria?	Yes	Yes	Yes	Yes	Yes	Yes	Yes	Yes

According to Table 14, the highest standard deviation of the factored combined stresses is observed at B2'. With 14 time series of the factored stresses generated and rain flow counting applied, BV’s SN curve for the combined stresses can be used to calculate the corresponding fatigue damages. It is noted that the highest standard deviation of the factored combined stresses occur at B2’.

7.5.5 Resultant OPB/IPB/TT fatigues

Following the outlined procedure, the combined fatigue analysis for OPB/IPB/TT involves applying rain flow counting and utilizing BV's SN curve for combined stresses, as elaborated in Section 2.25. These calculations are performed across all wave scatter diagrams presented in Section 4.2, ensuring comprehensive coverage of stress variations and their impact on fatigue life.

The results of the OPB/IPB/TT combined fatigues are detailed in Tables 15(a) and 15(b). It is noteworthy that the analysis reveals the lowest observed fatigue life of 1,263 years for ML 5. This finding demonstrates a significant margin of safety, as it surpasses the design criteria of 75 years by a substantial margin.

8. Discussions

A thorough and extensive approach to fatigue analysis has been detailed, highlighting the critical implications of Vortex-Induced Motion (VIM) and Out of Plane Bending/In Plane Bending (OPB/IPB) on mooring fatigue damages. Through comprehensive investigations and data analysis, it has been established that both VIM-induced and OPB/IPB-induced fatigues play pivotal roles in determining the fatigue life of the mooring system.

In-depth discussions in this section reveal the influence of these fatigue mechanisms. Detailed examination of the stress distributions, fatigue life predictions, and mitigation strategies stress the significance of addressing these challenges in mooring system designs.

8.1 VIM model test scale

In the early 2000s, there was a prevailing hypothesis in the offshore engineering industry that Reynolds numbers played a critical role in VIM tests, influencing the accuracy and applicability of model-scale results to full-scale offshore structures. This hypothesis spurred several Joint Industry Projects (JIPs) aimed at investigating the relationship between Reynolds numbers (model scales) and VIM response characteristics.

However, empirical findings from these studies challenged the initial belief. Specifically, tests conducted for semisubmersible platforms at different scales (small-scale at 1:160 and large-scale at 1:54) revealed remarkably consistent results in terms of VIM behavior (Zou *et al*. 2013, 2014). This meant that the size of the model, and consequently the Reynolds number range it represented, did not significantly alter the fundamental VIM patterns observed.

Similar observations were documented for Spar platforms in studies by Finnigan and Roddier (2007) and Roddier *et al*. (2009). These studies showed that the VIM response characteristics observed in both small-scale and large-scale model tests were highly comparable, further underscoring that Reynolds numbers did not exert a pronounced influence on the VIM test results.

Overall, these findings have provided valuable insights into the scaling laws and have prompted further investigation into other significant factors influencing overly conservative VIM test results for mooring fatigue analysis. These insights emphasize the importance of refining and optimizing VIM testing methodologies to better reflect real-world conditions and improve the accuracy of mooring system fatigue assessments.

8.2 VIM model test setup

VIM is characterized by resonant low-frequency responses that are highly sensitive to damping of the system. The presence or absence of damping significantly affects the magnitude of VIM motions observed. A practical method proposed by Zou *et al*. (2011) provides a simplified approach to quantify the damping effects that are typically neglected, specifically those from moorings and risers.

Further investigations by Zou *et al*. (2014) revealed the criticality of including these damping effects in VIM tests, especially for ultra-deepwater semisubmersible platforms. Their findings emphasized that neglecting mooring and riser damping can lead to unrealistically high VIM resonant responses, potentially penalizing mooring sizing and leading to high mooring material costs as well as transportation and installation costs.

Recognizing this issue, the Research Partnership to Secure Energy for America (RPSEA) initiated a project in 2015-2016 aimed at integrating damping effects into VIM tests. This effort presented by Sterenborg *et al.* (2016), demonstrating that implementing damping mechanisms reduced VIM motions by over 60% in nominal A/D under conditions of 25% equivalent linear damping.

The introduction of a linear actuator for an active damping system in VIM testing in 2016, marked a milestone. This system was further advanced and enhanced to not only introduce linear damping, but also recognize the quadratic damping in a world-class semisubmersible platform VIM test at the end of 2022 (Koop *et al.* 2024). While specific details of these advancements remain confidential due to contractual agreements, their implementation has enhanced the realism and reliability of VIM testing protocols.

For mooring fatigue analysis, it is crucial to adopt realistic VIM curves that account for the damping effects from moorings and risers. The preferred approach includes implementing linear + quadratic damping during VIM tests to ensure that design curves accurately reflect real-world conditions.

8.3 Characteristics of OVT movements

The mooring arrangement depicted in Fig. 1 illustrates a sophisticated mechanism designed to manage tensions and movements effectively.

The main housing is connected to the OVT foundation through a vertical rotation pin, allowing the entire OVT mooring tensioner to rotate in horizontal plane while the latch housing connects to the main housing via a horizontal-oriented pin, enabling vertical movements in the vertical plane.

Two key dimensions are important to this system:

1) *Vertical Pin to FPS Column*: this distance determines the reach of mooring line loadings (forces and moments) passing to the hull and allowing the mooring line to pivot around the vertical pin relative to the Floating Production System (FPS) column.
2) *Horizontal Pin to Chain Stopper*: this distance governs the vertical movements of the latch housing. The chain stopper is located within latch housing.

These two arms are equipped with low-friction bearings that ensure any rotations in the mooring line relative to the hull translate into movements within the articulation mechanism, rather than causing sliding between the chain links.

The system is designed with sufficiently low sliding moment limits at both the vertical and horizontal pins. This ensures that all chain links, starting from the first one, remain in a locked mode. This means there is no sliding movement occurring between adjacent chain links, even under varying tensions and movements of the mooring line.

Typical bearing friction ranges from 0.05 to 0.15 while the friction coefficient between two adjacent chains in seawater is higher, typically around 0.3. This difference in friction coefficients means that the maximum OPB/IPB moments experienced by the chain links are effectively controlled and constrained within allowable limits. This design approach optimizes the performance and reliability of the mooring system under various operational conditions in offshore environments.

8.4 Number of top chain links to be modelled individually

BV Guidelines (2014) recommend that for OPB/IPB analysis, individual modeling of the top 20 chain links is suggested. However, analysis results in section 7.5.1 have shown that the standard deviations of OPB/IPB moments at chain link #1 are significantly larger compared to those at chain link #3, by factors of 5.1 and 6.3, respectively. This indicates that the variability or significance of these moments decreases sharply along the chain.

Given this observation, modeling all 20 individual chain links for OPB/IPB analysis may be deemed excessive and unnecessary. Instead, it is recommended to represent the effects of the remaining top chain links (beyond the first few) using one equivalent element. This approach consolidates the modeling effort while still capturing the essential characteristics of OPB/IPB moment dynamics.

Here's a breakdown of key considerations:

- *Equivalent Representation*: the effects of the top chain links, such as their mass, stiffness, damping, and other relevant parameters, can be effectively represented by a single equivalent element. This simplifies the analysis without compromising accuracy significantly.
- *Pinned Boundary Condition*: modeling assumes a pinned boundary condition between adjacent chain links. This means that each link is connected in a way that allows rotation at the connection point, simulating realistic behavior under loading conditions.
- *Interlink Angle*: the interlink angle between adjacent chain links decreases gradually as you move down from the top chain. This angle progressively diminishes, approaching zero after the first 20 links.

By adopting this approach, one ensures that the analysis remains computationally feasible while capturing the essential dynamics and behaviors of the mooring system. It balances the need for detailed modeling with practical considerations of complexity and computational efficiency, adhering to best practices outlined in BV Guidelines (2014) for OPB/IPB analysis in mooring systems.

8.5 Coupled time domain dynamic analysis for OPB/IPB moments

In sections 7.5.2 and 7.5.3, significant coupling effects between platform motion modes (such as surge, sway, heave, roll, pitch, and yaw) and OPB/IPB moments have been observed and documented. These coupling effects imply that changes in platform motion modes influence the OPB and IPB moments, and vice versa. This interdependence complicates the analysis and suggests that simplifications or linearization in mooring combined stress analysis may not sufficiently capture the true dynamic interactions.

To ensure accurate assessment:

- *Dynamic Analysis Requirement*: it is recommended to evaluate mooring combined stress analysis from a comprehensive coupled time-domain dynamic analysis. This involves considering the full coupling effects between platform motions and mooring line responses, which influence OPB and IPB moments.
- *Time Domain Analysis for Hot Spots*: the stresses at critical locations (hot spots) along the mooring lines should be analyzed in the time domain. This approach requires post-processing

of time series data obtained from mooring analyses, where OPB and IPB stresses are evaluated separately and recombined based on Eq. (7).

8.6 Magnitudes of OPB and IPB stresses

OPB stress and IPB stress can be calculated from Eq. (9) below.

$$\Delta\sigma_{OPB} = \frac{16\ \Delta M_{OPB}}{\pi {d_{corroded}}^3} \quad \text{and} \quad \Delta\sigma_{IPB,studless} = \frac{2.33\ \Delta M_{IPB}}{\pi {d_{corroded}}^3} \tag{9}$$

In Eq. (9), $d_{corroded}$ is the corroded chain diameter.

Based on Eq. (9), which describes the stress changes (Δσ) due to OPB and IPB moments on the chain, the following observations have been noticed:

- *Magnitude of Moments*: although the magnitudes of OPB and IPB moments at chain link #1 are similar (as observed from Figs. 18 and 19), the resulting stresses are significantly different.
- *Stress Calculation*: OPB stress and IPB stress can be calculated from Eq. (9).
- *Stress Comparison*: despite similar moment magnitudes, the OPB stress is approximately 6.87 times larger than that of IPB stress. This disparity arises because the stress calculation for OPB involves a higher factor (16) compared to IPB (2.33).
- *Implications for Combined Stresses*: when evaluating the combined stresses in the mooring chain, particularly at chain link #1, the contribution from OPB stresses will dominate over IPB stresses due to the higher factor in Eq. (9).
- *Design Considerations*: one needs to ensure that the mooring components, including chain links and connections, are designed to withstand these different stress types adequately. Moreover, proper stress concentration factors given in Table 1 should be factored into the design to account for the combined stress fatigue.

8.7 Characteristic of the factored combined stresses at hot spots

The Eq. (7) describes the combinations of stresses to capture the worst-case scenarios at different hot spots (A, B, B', C) in the mooring system.

- *Phase Differences and Symmetry Planes*: each chain link typically has two symmetry planes, and there are phase differences among the stresses induced by OPB, IPB, and TT loads. These phase differences are critical because they affect how stresses combine and interact within the mooring chain links.
- *Combinations for Hot Spots*: to determine the worst-case combined stresses at critical locations (hot spots A, B, B', C), Eq. (7) specifies four possible combinations for hot spots B, B', and C, considering the contributions from OPB stresses, IPB stresses, and TT stresses. These combinations are crucial for assessing the maximum stresses that the mooring components may experience.
- *Hot Spot A Specifics*: at hot spot A, there are only two combinations described in Eq. (7) because OPB stresses do not contribute to the combined stresses (see Table 1). In this case, the combined stresses are primarily influenced by TT stresses and potentially IPB stresses, depending on their magnitude and phase relationship.
- *Standard Deviation Variations*: from Table 14, it is observed that the standard deviations of the combined stresses vary significantly (ranging from 26% to 45%) at hot spots B, B', and

C. This variation indicates the sensitivity of these locations to different loading conditions and the interactions between OPB, IPB, and TT stresses. In contrast, the standard deviations at hot spot A remain relatively consistent because TT stresses dominate and IPB stresses have minimal impact on the combined stresses.

- *Design Considerations*: these findings underscore the importance of comprehensive stress analysis in mooring design. One must accurately assess and combine the effects of OPB, IPB, and TT loads to ensure that the mooring system components are designed to withstand the highest possible stresses at critical locations (hot spots). Proper consideration of phase differences and symmetry planes is essential for capturing realistic stress scenarios and optimizing the design for durability and safety.

9. Conclusions

The holistic approach presented in the paper integrates various factors affecting mooring chain fatigue, emphasizing the critical role of realistic VIM curves and the combined stresses analysis. The conclusions provide insights into optimizing mooring system design to enhance durability, safety, and cost-effectiveness under operational conditions. The main findings are summarized and highlighted as follows:

- *Fatigue from Wave Scatter Diagrams*: the fatigue analysis based on wave scatter diagrams indicates that mooring chain fatigue due to this factor is not critical. This suggests that the design criteria based on wave-induced fatigue are adequately met.
- *Vortex-Induced Motion (VIM) Fatigue*: VIM-induced mooring chain fatigue emerges as a critical issue. It is emphasized that using realistic VIM curves for mooring fatigue analysis is crucial. This ensures that the predicted fatigue damages align closely with actual operational conditions, where VIM effects can significantly impact fatigue life.
- *Single Event Fatigue Analysis*: single events such as 100-year hurricanes and 100-year loop/eddy currents were analyzed. It was found that fatigue damages due to 100-year hurricanes are less severe compared to those induced by 100-year loop currents when employing normal VIM curves. This comparison serves as a robust check to understand the relative impacts of different extreme events on mooring chain fatigue.
- *Max VIM Curves and Worst Current Direction*: considering maximum VIM curves along with the worst current direction leads to predictions that mooring chains #5 to #8 and #13 to #16 don't satisfy the design criteria. However, it is noted that such an approach is overly conservative and beyond practical operational scenarios.
- *Combined Stresses (OPB/IPB/TT) Fatigue*: fatigue damages due to the combined stresses from OPB, IPB, and TT are highlighted as a significant contributor to mooring chain fatigue. Effective design strategies such as adopting OVT are crucial in mitigating these combined stresses and reducing their impact to non-governing levels.

Major recommendations for mooring chain fatigue analysis are outlined as follows,

- *Adoption of Realistic VIM Curves*: it is crucial to adopt realistic VIM curves for mooring fatigue analysis. These curves should ideally be derived from VIM tests that incorporate damping effects (preferably linear and quadratic damping) due to moorings and risers. These design curves have a significant impact on mooring fatigue, particularly in regions with strong and steady loop currents.

- *Modelling of OVT Geometry*: proper modelling of the OVT geometry and its components is essential for accurate OPB/IPB fatigue analysis. This includes detailed considerations such as the dimensions of the OVT foundation, connections with the hull column, dimensions of the main housing and latch housing, vertical and horizontal pin diameters, distances to the hull column, and the friction characteristics at both the vertical and horizontal pins. These parameters influence the distribution and magnitude of OPB/IPB moments on the mooring chain links, impacting fatigue life assessments.
- *Optimized Chain Link Modelling*: based on the findings discussed in Section 8.4, it is recommended to model only the top three chain links individually. The remaining 17 top chain links can be effectively represented by one equivalent element. This approach balances computational efficiency with accuracy, ensuring that the essential characteristics of the mooring chain's behavior are captured without excessive detail.
- *Coupled Time Domain Dynamic Analysis*: as highlighted in Section 8.5, employing coupled time domain dynamic analysis is strongly recommended. This approach integrates the effects of platform motions, environmental loads (such as wind, waves and currents), and mooring/riser system dynamics in a interacting manner. It ensures that the interactions and couplings between different modes of motion and loads are accurately accounted for, yielding more reliable predictions of fatigue damage and overall system performance.

By following these recommendations, the mooring design and fatigue analysis can be conducted with enhanced accuracy and reliability, aligning closely with operational conditions and ensuring the durability and safety of the mooring system under various environmental scenarios.

Acknowledgments

The research presented in this paper received financial support from Floating and Green Energy Consulting, LLC. This organization is committed to advancing fundamental research and development initiatives aimed at both the oil and gas industry and renewable energies sectors. Their support facilitated the comprehensive analysis and findings detailed in this study, contributing to advancements in understanding mooring chain fatigue.

References

ABS Guidance Notes (2021), *The Application of Fiber Rope for Offshore Mooring*, American Bureau of Shipping, Spring, TX, USA.

ABS Guide (2023), *Position Mooring Systems*, American Bureau of Shipping, Spring, TX, USA.

API RP 2MET (2021), *Derivation of Metocean Design and Operating Conditions*, American Petroleum Institute, USA.

API RP 2SK (2008), *Design and Analysis of Stationkeeping Systems for Floating Structures*, American Petroleum Institute, USA.

API RP 2SM (2001), *Recommended Practice for the Design, Manufacture, Installation and Maintenance of Synthetic Fiber Ropes for Offshore Moorings*, American Petroleum Institute, USA.

API RP 2T (2010), *Recommended Practice for Planning, Designing and Constructing Tension Leg Platforms*, American Petroleum Institute, USA.

Bureau Veritas Guidance Note NI 604 DT R00 E (2014), *Fatigue of Top Chain of Mooring Lines due to In-plane and Out of-plane Bendings*, Marine & Offshore Division, 92571 Neuilly sur Seine Cedex, France.

Chung, W.C., Kang, H.Y. and Kim, M.H. (2020), "Multi-scale approach of a chain-mooring OPB-induced failure considering time-varying interlink bending stiffness and fairlead condition", *Appl. Ocean Res*., **98**, 102128. https://doi.org/10.1016/j.apor.2020.102128.

Das, S. and Zou, J. (2015), "Characteristic responses of a dry tree paired-column and dDeep draft semisubmersible in central Gulf of Mexico", *Proceedings of the 20th SNAME Texas Section Offshore Symposium*, Houston, USA, February.

DNV-OS-E301 (2021), *Position Mooring*, Det norske Veritas, Høvik, Norway.

DNV-RP-C203 (2016), *Fatigue Design of Offshore Steel Structures*, Det norske Veritas, Høvik, Norway.

D'Souza, R.B., Basu, S., Bhaumik, T. and Sharples, M. (2019), "The Semisubmersible Floating Production System: A 25-Year Technical and Historic Retrospective", *Proceedings of the SNAME Maritime Convention 2019*, Tacoma, Washington, USA, October.

D'Souza, R.B.; Zou, J., Jatar, S.M. and Andersen, D.B. (2024), "Gulf of Mexico Deepwater Mooring Experience Applied to Floating Offshore Wind Turbines", *Accepted and will be published in SNAME Maritime Convention 2024*, Norfolk, VA, USA, October.

Finnigan, T. and Roddier, D. (2007). "Spar VIM model tests at supercritical reynolds numbers", *Proceedings of the International Conference on Offshore Mechanics and Arctic Engineering*, San Diego, California, USA.

Gonçalves, R., Rosetti, G., Fujarra, A.C. and Oliveira, A. (2012), "Experimental study on vortex-induced motions of a semi-submersible platform with four square columns, Part I: Effects of current incidence angle and hull appendages", *Ocean Eng*., **54**(4), 150-169. https://doi.org/10.1016/j.oceaneng.2012.06.032.

Gordon, R.B., Brown, M.G. and Allen, E.M. (2014), "Mooring integrity management: A state-of-the-art review", *Proceedings of the Offshore Technology Conference*, Houston, TX, USA, May.

Izadparast, A., Heyl, C., Ma, KT; Vergas, P. and Zou, J. (2018), "Guidance for assessing out-of-plane bending fatigue on chain used in permanent mooring systems", *Proceedings of the 23rd SNAME Texas Section Offshore Symposium*, Houston, USA, February.

Koop, A., Leverette, S., Bangs, A., Withall, T., Castillo Valverde, F., Zanden, J.V.D., Heerink, R. and Wilde, J.D. (2024), "Investigating the effect of damping originating from mooring and risers on the VIM response of a semi-submersible floater using coupled CFD-time-domain simulations", *Proceedings of the Offshore Technology Conference*, Houston, TX, USA, May.

Kvitrud, A. (2013), "Failures in anchor lines and methods for improving the safety level", *Proceedings of the Normoor Conference*, Høvik, Norway, November.

Ma, K.T., Duggal, A., Smedley, P., L'Hostis, D. and Shu, H. (2013), "A historical review on integrity issues of permanent mooring systems", *Proceedings of the Offshore Technology Conference*, Houston, TX, USA, May.

Ma, W., Wu, G., Thompson, H., Prislin, I. and Maroju, S. (2013), "Vortex induced motions of a column stabilized floater", *Proceedings of the Deep Offshore Technology International Conference*, Houston, TX, USA.

Melis, C., Jean, P. and Vargas, P. (2005), "Out of plane bending testing of chain links", *Proceedings of the International Conference on Offshore Mechanics and Arctic Engineering*, Halkidiki, Greece.

Rampi, L., Bignonnet, A., Le Cunff, C., Bourgin, F. and Vargas, P. (2016a), "Chain out of plane (OPB) fatigue joint industry project (JIP) FEA results and multiaxiality study results", *Proceedings of the International Conference on Offshore Mechanics and Arctic Engineering*, Busan, South Korea.

Rampi, L., Gerthoffert, A., Francois, A., Bignonnet, A. and Vargas, P. (2016b), "Chain out of plane (OPB) fatigue joint industry project (JIP) fatigue test program results and methodology", *Proceedings of the International Conference on Offshore Mechanics and Arctic Engineering*, Busan, South Korea.

Rampi, L., Dewi, F., Francois, M., Gerthoffert, A. and Vargas, P. (2016c), "Chain out of plane (OPB) fatigue joint industry project (JIP) static test program and OPB interlink stiffness", *Proceedings of the International Conference on Offshore Mechanics and Arctic Engineering*, Busan, South Korea.

Rampi, L., Dewi, F. and Vargas, P. (2015), "Chain out of plane bending (OPB) joint industry project (JIP) summary and main results", *Proceedings of the Offshore Technology Conference*, Houston, TX, USA, May.

Rampi, L. and Vargas, P. (2006), "Fatigue testing of out of plane bending mechanism of chain links", *Proceedings of the International Conference on Offshore Mechanics and Arctic Engineering*, Hamburg, Germany.

Roddier, D., Finnigan, T. and Liapis, S. (2009), "Influence of the reynolds number on spar vortex induced motions (VIM): Multiple scale model test comparisons", *Proceedings of the International Conference on Offshore Mechanics and Arctic Engineering*, Honolulu, HI, USA.

Sai, M. and D'Souza, R.B. (2013), "Application of lessons learned from field experience to design, installation and maintenance of FPS moorings", *Proceedings of the Offshore Technology Conference*, Houston, TX, USA, May.

Sterenborg, J., Koop, A., de Wilde, J., Vinayan, V., Antony, A. and Halkyard, J. (2016), "Model test investigation of the influence of damping on the vortex induced motions of deep draft semisubmersibles using a novel active damping device", *Proceedings of the International Conference on Offshore Mechanics and Arctic Engineering*, Busan, Korea.

Zou, J. (2008), "Dynamic responses of a dry tree semi-submersible platform with ram style tensioners in the post-Katrina irregular seas", *Proceedings of the International Society of Offshore and Polar Engineering Conference*, Vancouver, Canada.

Zou, J. (2014), "VIM response of a dry tree pair-column semisubmersible platform and its effects on mooring fatigue", *Proceedings of the 19th SNAME Texas Section Offshore Symposium*, Houston, USA, February.

Zou, J., Poll, P., Antony, A., Das, S., Padmanabhan, P., Vinayan, V. and Parambath, A. (2014), "VIM Mmodel testing and VIM induced mooring fatigue of a dry tree paired-column semisubmersible platform", *Proceedings of the Offshore Technology Conference*, Houston, TX, USA, May.

Zou, J., Poll, P., Park, Y.C., Converse, R., Antony, A. and Moideen, H. (2011), "The gulfstar standard floater and its vortex induced motion model tests", *Proceedings of the International Society of Offshore and Polar Engineering Conference*, Maui, HI, USA.

Zou, J., Poll, P., Roddier, D., Tom, N. and Peiffer, A. (2013), "VIM Testing of a Paired Column Semisubmersible", *Proceedings of the International Conference on Offshore Mechanics and Arctic Engineering*, Rotterdam, Nantes, France.

MK